THE DEVELOPMENT OF AN IN VITRO FLOW SIMULATION DEVICE TO STUDY THE EFFECTS OF ARTERIAL SHEAR STRESS PROFILES ON ENDOTHELIAL CELLS

A Thesis
Presented to
The Academic Faculty

by

Sarah Elizabeth Coleman

In Partial Fulfillment
of the Requirements for the Degree
Masters of Engineering in
Biomedical Engineering

Georgia Institute of Technology and Emory University

August 2005

THE DEVELOPMENT OF AN IN VITRO FLOW SIMULATION DEVICE TO STUDY THE EFFECTS OF ARTERIAL SHEAR STRESS PROFILES ON ENDOTHELIAL CELLS

Approved by:

Hanjoong Jo, Ph.D., Advisor
College of Engineering
Georgia Institute of Technology

Don P. Giddens, Ph.D.
Dean, College of Engineering
Georgia Institute of Technology

Ajit P. Yoganathan, Ph.D.
College of Engineering
Georgia Institute of Technology

W. Robert Taylor, M.D., Ph.D.
College of Engineering
Georgia Institute of Technology

Date Approved: May 25, 2005

ACKNOWLEDGEMENT

I would like to thank the following people for there help throughout my time in graduate school:

Dr. Jo, for many things, but most of all for always being on my side,

My committee members: Don P. Giddens, Ph.D., Ajit Yoganathan, Ph.D., and W. Robert Taylor, M.D., Ph.D. for there time and guidance,

My mom, for wanting me to be happy,

My dad, for never letting me give up,

Manu and the "Rainbow Coalition," without whom I might not have made it, and definitely would not have had as much fun,

and Trey, for your patience, support, love, and understanding.

TABLE OF CONTENTS

LIST OF TABLES

LIST OF FIGURES

LIST OF ABBREVIATIONS

AG – Atheroprone Shear Profile
AP – Atheroprotective Shear Profile
BC – Boundary Condition
BMP-4 – Bone Morphogenic Protein-4
BSA – Bovine Serum Albumin
CFD – Computational Fluid Dynamics
cSt - Centistokes
CVD – Cardiovascular Disease
dyn/cm^2 – Dynes per square centimeter
EC – Endothelial Cell
ECM – Extracellular Matrix
eNOS – Endothelial Nitric Oxide Synthase
FBS – Fetal Bovine Serum
Hz - Hertz
ICAM-1 – Intercellular Adhesion Molecule-1
LDL – Low-Density Lipoprotein
LDV – Laser Doppler Velocimetry
MAEC – Murine Aortic Endothelial Cells
MMP – Matrix Metalloproteinase
$NO^{\cdot}$ – Nitric Oxide
OLS – Oscillatory Laminar Shear
oxLDL – Oxidized Low-Density Lipoprotein
PBS – Phosphate Buffered Saline
PDGF – Platelet Derived Growth Factor
PECAM – Platelet Endothelial Cell Adhesion Molecule
r – Cone Radius
Ř – Dimensionless Parameter
rev/s – Revolutions per second
ROS – Reactive Oxygen Species
RT – Room Temperature
SMC – Smooth Muscle Cells
SDS – Sodium Dodecyl Sulfate
SDS-PAGE – SDS-Polyacrylamide Gel Electrophoresis
SSRE – Shear Sensitive Response Element
TF – Tissue Factor
TGF-β – Transforming Growth Factor-β
ULS – Uni-directional Laminar Shear
VCAM – Cascular Cell Adhesion Molecule
WCL – Whole Cell Lysate
α - Cone Angle
μ - Viscosity
ν – Kinematic Viscosity
ω – Angular Velocity

SUMMARY

Mechanical forces are important regulators of cell function in many tissues including, for example, bone and components of the cardiovascular system. The endothelial lining of blood vessels has been shown to respond in an atheroprotective manner to unidirectional, laminar flow-induced shear stress and in an atherogenic manner to oscillating and low levels of shear. We have developed a cone and plate shear apparatus to simulate fluid shear stress on endothelial cells *in vitro*. The significant feature of this apparatus is that, unlike other *in vitro* flow systems, it accurately produces varying levels of shear stress, consistent with those created *in vivo* during the cardiac cycle. Flow characteristics of this system were verified by computational fluid dynamics (CFD) and laser Doppler velocimetry (LDV). Cellular responses were monitored by cell morphology and protein expression. These responses are consistent with *in vivo* responses as well as previous work using other *in vitro* flow systems.

CHAPTER 1

Introduction and Background

Atherosclerosis

Over the last decade, heart disease was the leading cause of death, disability, and healthcare expense in the United States [1] and was noted as the leading cause of worldwide deaths in the 1990s. [2] The estimated direct and indirect cost of cardiovascular disease in the United States is projected to be $393.5 billion in 2005. [3] The cardiovascular disorder responsible for the rise in cardiovascular-related mortality is ischemic heart disease, which is usually caused by atherosclerosis. The upward trend of ischemic heart disease cases is expected to continue due to the aging of the population, explosion of obesity and diabetes and the lack of physical activity. [1]

Atherosclerosis, a disease of the large and medium-sized arteries, is the chief cause of death in the US and most of the western world. Severe atherosclerosis interferes with blood flow; this is particularly important for the heart and brain, with the result being myocardial or cerebral ischemia or even a myocardial infarction or stroke. However even in the early stages of the disease, before an atherosclerotic lesion may occlude blood flow, there is believed to be an important relationship between the characteristics of blood flow in arteries the disease process.

For a large artery, the vessel wall is composed of three distinct layers: an intima, a media, and an adventia. Under normal conditions, the intima is composed of little more than the endothelial monolayer and a basement membrane. The media is composed of vascular smooth muscle cells together with extracellular matrix, primarily collagen and elastin. The

adventitia is the strong outer layer and is composed of fibroblasts, connective tissue, collagen, and elastin.

A key characteristic of lesion-prone regions is intimal thickening. This thickening of the intima is due to the migration and proliferation of vascular smooth muscle cells, originating from the vessel media. [4, 5] The degree of intimal thickening has been found to correlate with the measures of the hemodynamic environment, including oscillatory shear index. [6, 7] This provides an important piece of evidence as to the important role of hemodynamics in the disease process.

The earliest changes that precede the formation of atherosclerotic lesions take place in the endothelium. These include increased endothelial permeability to lipoproteins and other plasma constituents, up-regulation of leukocyte adhesion molecules, up-regulation of endothelial adhesion molecules, and migration of leukocytes into the artery wall, as shown in Figure 1. In persons with hypercholesterolemia, the influx of these cells follows the extracellular deposition of amorphous and membranous lipids. [8] Possible causes of endothelial dysfunction leading to atherosclerosis include elevated and modified low-density lipoprotein (LDL); free radicals caused by cigarette smoking, hypertension, and diabetes mellitus; disturbed regions of flow; genetic alterations; elevated plasma homocysteine concentrations; infectious microorganisms such as herpes viruses or *Chlamydia pneumoniae*; and combinations of these or other factors. [4, 9]

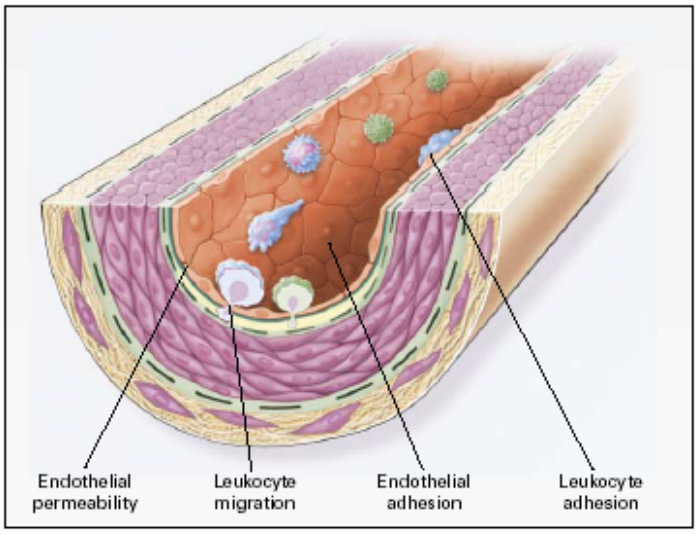

Figure 1. Initial Stages of Atherosclerosis (image from Ross, R., 1999.)

As shown in Figure 2, the next stage in the progression of atherosclerosis is the formation of fatty streaks. This type of lesion may be present throughout a person's lifetime and is common in infants and young children. [8] Fatty streaks initially consist of foam cells (macrophages containing lipids) together with T lymphocytes. Later, smooth muscle cells also appear in the fatty streak. The steps involved in this process include smooth muscle cell migration, T-cell activation, foam cell formation, and platelet adherence and aggregation. If these responses continue, they can thicken the artery wall. The artery then compensates by gradual dilation so that up to a point the lumen remains unaltered. This is known as vessel wall remodeling. [10]

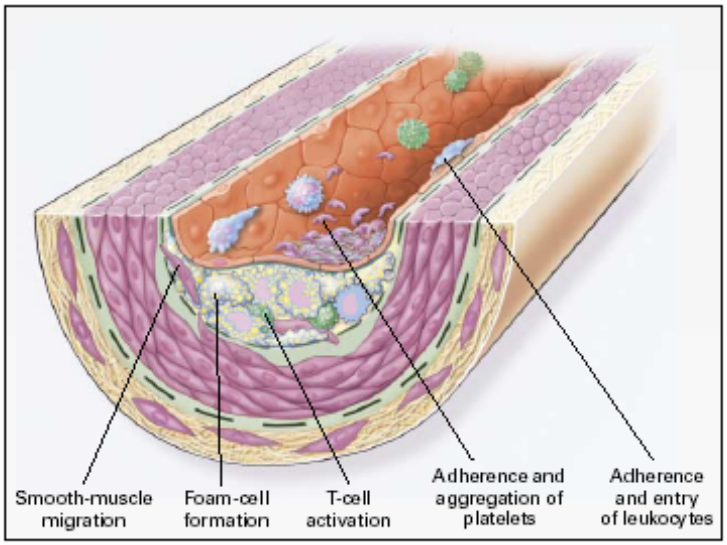

Figure 2. Fatty Streak Formation (image from Ross, R., 1999.)

As fatty streaks progress to intermediate and advanced lesions, they tend to form a fibrous cap that separates the lesion from the lumen (see Figure 3). This represents a type of healing or fibrous response to the injury. The fibrous cap covers a mixture of leukocytes, lipid, and debris, which may form a necrotic core. These lesions expand at their shoulders due to continued leukocyte adhesion and entry. The necrotic core represents the result of apoptosis and necrosis, increased proteolytic activity, and lipid accumulation. At some point the artery can no longer compensate by dilation; the lesion may then intrude into the lumen and alter the flow of blood.

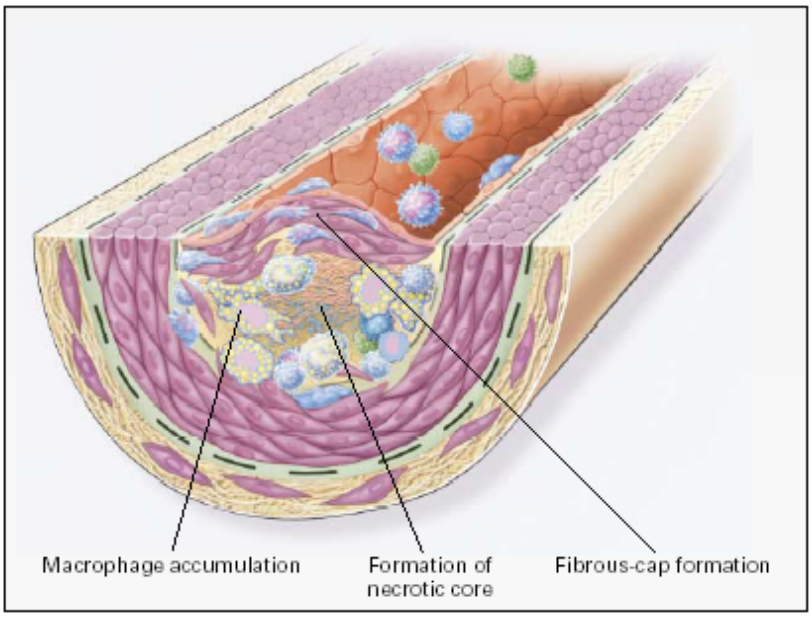

Figure 3. Advanced Atherosclerotic Lesion (image from Ross, R., 1999.)

Rupture of the fibrous cap, as seen in Figure 4, or ulceration of the fibrous plaque can rapidly lead to thrombosis and usually occurs at sites of thinning of the fibrous cap that covers the advanced lesion. Thinning of the fibrous cap is apparently due to the continuing influx and activation of macrophages, which release matrix metalloproteinases (MMPs) and other proteolytic enzymes at these sites. These enzymes cause degradation of the matrix, which can lead to hemorrhage from the *vasa vasorum* or from the lumen of the artery and can result in thrombus formation and occlusion of the artery.

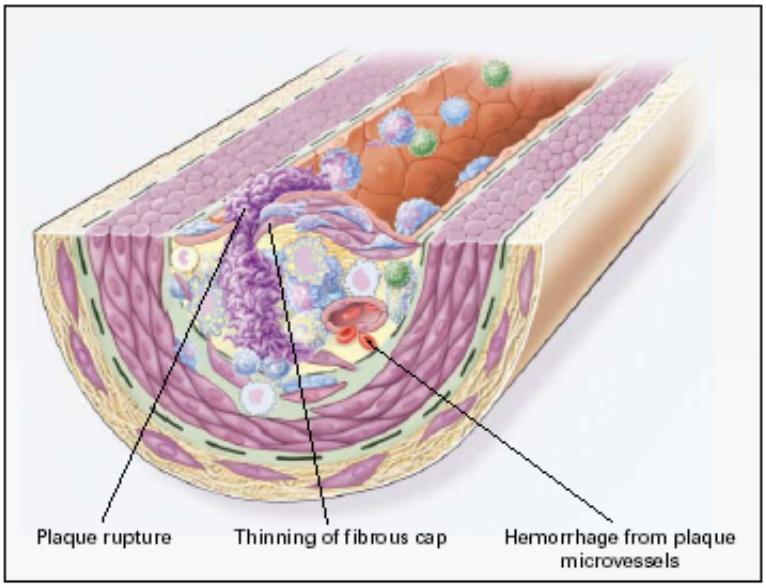

Figure 4. Unstable Plaque (image from Ross, R., 1999.)

Hemodynamics

The pulsatile flow of blood through the branched arterial vasculature generates various types of hemodynamic forces - hydrostatic pressures, cyclic strains, and wall shear stresses - that can impact vessel wall biology. Hydrostatic pressure is the normal force exerted on the vessel wall due to the pressure of the blood. Changes in pressure during the cardiac cycle cause the vessel wall to stretch, which results in cyclic strain of the vessel wall, specifically the basement membrane. Fluid shear stress is the tractive force (acting tangentially to the blood vessel) produced by a moving viscous fluid on a solid body constraining its motion. Its magnitude increases with fluid velocity and with viscosity. Near a plane boundary, the fluid velocity increases linearly with distance from the surface and the shear stress may be computed from the Newton's equation,

$$\tau = \mu \frac{dv}{dz} \quad (1)$$

where τ is wall shear stress
μ is viscosity
dv/dz is the velocity gradient.

Typical average values of shear in the major human arteries are 2-20 dyn/cm^2, with localized increases to 30-100 dyn/cm^2 near arterial branches and regions of sharp wall curvature. [11]

Blood flow patterns can vary in complexity from the relatively uniform, well-developed laminar patterns that occur in the unbranched portions of medium-sized muscular arteries to the complex disturbed flow patterns that result from significant wall shear stress gradients over relatively short distances at branch points and significant curves in the vasculature. [12, 13] These complex flow patterns involve regions of flow separation, [14] recirculation, and reattachment that generate oscillatory wall shear stress.

Shear Stress and Atherosclerosis

Over the last several decades attention has been focused on the detailed characteristics of blood flow as a localizing factor in atherosclerosis. Specific arterial sites such as branches, bifurcations and curvatures cause characteristic alterations in the flow of blood, including oscillatory flow, decreased shear stress, and increased turbulence. [15] These disturbed flow patterns are typically associated with the early appearances and subsequent progression of atherosclerotic lesions. In contrast, the unbranched, straight portions of arteries that carry uniform laminar flow are relatively protected from atherogenesis. For many years it has been believed that low shear areas (e.g. the complex geometries where the time-averaged wall shear stresses are small, due to forward-reverse

flow cycles) were especially atherosclerosis-prone, [16] whereas high shear areas (such as straight arteries) were relatively atherosclerosis-protected. [13]

Numerous studies have been conducted to determine the relationship between shear stress and arterial integrity. Fry [17] provided the first demonstration of endothelial damage by elevated shear forces. Krueger [18] made the first attempt to use cultured cells in an *in vitro* flow system. Rosen et al [19] and De Forrest and Hollis [20] demonstrated an increase in histamine synthesis with increasing shear stress. This first suggested that shear stress might play a role in mediating many of the biochemical and transport processes that occur *in vivo*.

The nature of flow (e.g. whether shear stress is high or low) appears to be important in determining whether lesions occur at these vascular sites. Changes in flow alter the expression of genes that have elements in their promoter regions that respond to shear stress, known as shear-sensitive response elements (SSRE). For example, the genes that code for intercellular adhesion molecule-1 (ICAM-1), [21] platelet-derived growth factor (PDGF), [22] and tissue factor (TF) [23] in endothelial cells (EC) have SSREs and their expression is increased or reduced by shear stress. [24] Rolling and adherence of monocytes and T-cells occur at these sites of low shear as a result of the upregulation of adhesion molecules on both the endothelium and leukocytes. This represents the beginning of an inflammatory response and is recognized as a key first step in the cascade of atherogenesis. Thus, alterations in blood flow appear to be critical in determining which arterial sites are prone to have lesions. [15, 25, 26]

It is now well accepted that uniform laminar shear stresses are characteristically associated with athero-protected arterial geometries *in vivo.* The biochemical events

observed in these regions have led to the hypothesis that this type of biomechanical stimulation (steady, laminar shear stress) acts to chronically upregulate the expression of a subset of atheroprotective genes (e.g. eNOS) in endothelial cells. These atheroprotective genes and associated proteins then act locally in the lesion-protected areas to offset the effects of systemic risk factors, such as hypercholesterolemia, hyperglycemia, and hypertension. Therefore, upregulation of atheroprotective genes by uniform laminar shear stress is a possible mechanistic link between the local hemodynamic environment, endothelial cell gene expression, and early events in atherogenesis. This hypothesis also conversely extends to regions of complex and disturbed flows that occur in lesion-prone arterial geometries. [27] These complex flows generate low and oscillatory shear stresses that stimulate the expression of pro-atherogenic genes (e.g. adhesion molecules, growth factors, and cytokines).

Shear Stress and Endothelial Cell Biology

Specific arterial sites such as branches, bifurcations, and curvatures cause characteristic alterations in the flow of blood, including decreased shear stress and increased turbulence. [15] At these sites, specific molecules form on the endothelium that are responsible for the adhesion, migration, and accumulation of monocytes and T-cells. Such adhesion molecules, which act as receptors for glycoconjugates and integrins present on monocytes and T-cells, include selectins, intercellular adhesion molecules, and vascular-cell adhesion molecules (V-CAM). [15] Molecules associated with the migration of leukocytes across the endothelium, such as platelet-endothelial-cell adhesion molecules (PECAM) [28]

act in conjunction with chemoattractant molecules generated by the endothelium, smooth muscle, and monocytes to attract T-cells and additional monocytes into the arterial wall. [29]

Among the cellular components of the arterial wall, it is the endothelium that has received most of the attention in the field of hemodynamics and atherosclerosis. This, at least in part, is due to its strategic location, positioned between the flowing blood and the underlying vessel wall. As an interface, it might be a mediator of any blood-associated effects on vascular biology, including those due to hemodynamics. Vascular endothelial lining *in vivo* is constantly subjected to fluid shear stresses resulting from normal and altered patterns of blood flow. The endothelium demonstrates a remarkable variety of responses to fluid shear stresses. The cells align with the flow direction, [11, 17, 27, 30] mobilize cytosolic free calcium, [31] activate ion channels, [32] organize internal cytoskeletal structures, [33, 34] and produce vasoactive molecules. [35-37] Confluent endothelial monolayers also divide in the presence of turbulent flow, while proliferation is inhibited in endothelial cells exposed to laminar shear. [38]

Minor changes in shear stress, on the order of 0.5 to 1.0 dyn/cm^2, can have significant influence on biological processes such as transmigration of leukocytes. [39] Unidirectional laminar flow protects endothelial cells from apoptosis, even at low shear stress levels, [40] and stabilizes the endothelial barrier function. [41] The endothelial cell, once thought to be a passive, non-thrombogenic barrier is now recognized as capable of being activated and synthesizing a variety of proteins. At the blood-arterial wall interface, it is acted on directly by the hemodynamic stress imposed by flowing blood. This stress has two components, a normal component - pressure and a tangential component - shear stress. The pressure is pulsatile and the endothelial cell both feels the pressure directly and senses the movement of

the basement membrane being cyclically stretched by the pressure changes. The endothelial cell also feels the wall shear stress associated with the pulsatile flow. [42-44] The possibility that hemodynamic forces can act directly as pathophysiologic stimuli for endothelial dysfunction helps to explain why the earliest lesions of atherosclerosis characteristically develop in a non-random pattern, the geometry of which correlates with branch points and other regions of altered blood flow. [45]

A number of *in vivo* observations suggest that hemodynamic forces can alter endothelial structure and function. [30, 46] These include the demonstration of increased macromolecular permeability, lipoprotein accumulation, endothelial cell damage and repair, leukocyte adhesion molecule expression, and mononuclear leukocyte recruitment near branch points and bifurcations, axial alignment (in the direction of flow) to laminar flow regions, and the disruption of this orderly pattern in regions of disturbed flow.

Some of the more acute shear-induced changes appear to involve regulation at the level of rate-limiting enzymes or substrate availability (e.g. nitric oxide (NO) production by nitric oxide synthase). However, in the case of delayed responses, in which protein synthesis is occurring, transcriptional upregulation of gene expression appears to be stimulated as a direct consequence of exposure to fluid mechanical forces.

At the present time, considerable attention is being focused on the question of the identity, location, and mechanisms of action of endothelial flow-sensitive mechanotransducers. Several distinct molecules (e.g. cell-surface ion channels, various receptor-associated G-proteins, and members of the mitogen-activated and stress-activated protein kinase cascades) are rapidly activated in response to fluid shear stresses applied to the endothelial cell surface. [14, 40] In addition, cellular components, such as the cytoskeleton,

plasma-membrane caveolae, lateral cell-cell junctional proteins, basal focal adhesion complexes, and even the lipid bilayer of the plasma membrane, also appear to be participating in shear-induced endothelial responses. [47] Finally, various second messengers, including ionized cytosolic calcium, intracellular lipid products of the polyphosphoinositide pathway, and NO are generated in the context of flow stimulation. As discussed by Davies, [14] the challenges to understanding the interaction of these spatially and temporally different components in the dynamic interaction of the endothelial cell's response to biomechanical stimulation are in sorting out where transmission becomes transduction, as well as cause and effect relationships.

What we do know is that shear stress alters NO release and that NO in turn influences leukocyte adhesion. [48] It also has been suggested that NO produced by endothelial cells may scavenge oxygen free radicals and in doing so provides protection to the vessel wall. [49] Taken together with the above noted influence of shear stress on NO release by endothelial cells, this is strongly suggestive of a link between hemodynamics and the oxidative environment of the vessel wall which is known to be important to mechanisms involved in the disease process. [50]

Cell culture experiments represent a model in which one can study specific mechanisms involved in endothelial biologic responses under well-defined flow conditions. However, the investigations of flow effects on cultured endothelial cells have focused on the effects of a steady laminar shear stress. These *in vitro* studies show that for a confluent monolayer of cultured cells, the application of physiological levels of shear stress causes a significant alteration in endothelial cell structure and function. Specifically, there are four results:

1. An elongation in the direction of flow, [11, 27]
2. A rearrangement of the actin microfilaments into stress fibers aligned with the direction of flow, [51], [52]
3. An influence on endocytotic processes, including the enhancement of the receptor-mediated binding, internalization, and degradation of LDL, [53, 54]
4. Alterations in the expression of a broad spectrum of pathophysiologically relevant genes including growth factors, such as PDGF-A and PDGF-B; transforming growth factor-β (TGF-β); fibrinolytic factors, such as tPA; and adhesion molecules, such as ICAM-1 and VCAM-1. [44]

In essence, geometry has important effects on the fluid mechanics within the vascular system, and the resulting local hemodynamic factors provide for the mechanical environment of the cellular participants. These hemodynamic factors, such as low and oscillating shear stress, then influence such basic atherogenic mechanisms as smooth muscle cell proliferation and migration into the intima, connective tissue synthesis, and monocyte/macrophage recruitment and the formation of foam cells.

CHAPTER 2

In Vitro Blood Flow Simulation

Introduction

Due to the complexity of the *in vivo* environment, systematic study of phenomena of cellular response to mechanical stimulation has relied heavily on the use of *in vitro* preparations. Such work has frequently involved cell culture systems with controlled delivery of a mechanical input such as fluid shear stress. Laboratory apparati devised for that purpose span a large range of sophistication, and they feature mechanical input signals of varied levels of precision, complexity and homogeneity.

Over the past twenty years, various models have been designed to simulate the effects of the blood flow environment on cultured endothelial cells in an effort to understand their response to biomechanical forces. These devices are designed to generate either a single type of stimulus (e.g. shear stress, hydrostatic pressure, hoop stress) or a combination of stimuli. [14] Models investigating the influence of shear stress alone on EC response have simulated steady laminar, [11] sinusoidal (net forward flow without reversing) and oscillatory, [55, 56] disturbed (i.e. spatial variation), [57] and turbulent (i.e. random temporal and spatial variations) flows. [38, 58] Results from these studies demonstrate the ability of the EC not only to sense shear stress stimuli but also to discriminate among distinct types of flow patterns. It is becoming more apparent that the exact nature of the flow stimulus *in vitro* regulates EC phenotype [59] and is hypothesized that the local hemodynamic environment *in vivo* can contribute to regional differences in EC phenotype. [60]

The most widely studied mechanotransduction system is the endothelial cell's response to fluid shear stress. [14] These cells line the lumen of the cardiovascular system and are continuously exposed to dynamic changes in flow rate within each cardiac cycle. In the human circulatory system, blood flow in arteries is highly dynamic and variable. For a typical waveform, the contraction of the heart during systole forces blood to accelerate through the arteries within 100-200 ms. As the heart expands to collect blood during diastole, arterial flow will decelerate in 200-300 ms, briefly reverse in direction, and then reverse again and continue distally to a low forward basal flow until the next cycle. The velocity characteristics of an arterial waveform (e.g. peak amplitude, flow reversal, pulsation frequency) are variable throughout the vasculature and are dependent on local geometry, elasticity of the artery wall, peripheral vascular resistance and heart rate. [61], [62] *In vitro* models exposing cells to hydrodynamic shear stress, such as the cone and plate, [11, 46] and the parallel plate flow chamber [27] have been used to elucidate the endothelial cell response to this type of mechanical stimuli. With few exceptions, the typical experiment involves so-called steady flow being applied to previously unstimulated cells.

The endothelial cells lining the branched tubular array of the arterial vasculature are subjected to a broad spectrum of flow patterns depending upon their location. Several studies using different *in vitro* model systems, clearly indicate that endothelial cells can sense differences in the temporal and/or spatial characteristics of flow and translate these biomechanical stimuli into different biological responses. For example, steady laminar flow appears to enhance endothelial survival by suppressing apoptosis [59] whereas turbulent flow can trigger endothelial cell division. [38] Differences in the temporal properties of laminar flow stimulation, generated by instantaneous (impulse) versus gradual (ramp) application of

the same level of shear stress, can elicit very different responses in endothelial gene expression. [63] Similarly, oscillatory versus steady laminar flow elicits marked differences in the pattern of adhesion molecule expression in cultured endothelium. [57]

In Vitro **Shear Systems**

Several special-purpose systems have been developed to deliver fluid shear stresses concurrently with substrate deformations, [64] such as a four-point bending system that modulates fluid shear stress (unquantified) independently of substrate strain by means of changing the thickness of substrate layer. [65] Another approach to combining fluid shear and substrate distention is to work with cultures growing on the inner wall of a highly distensible tube. [66] Since flow rate and hence shear stress depends on pressure gradient, whereas substrate distention (for a given external pressure) depends on absolute internal pressure, these two stimulus modes can be independently controlled. [67] The *in situ* rabbit iliac artery stretch/shear preparation developed by Ayajiki [68] functioned in an analogous manner (except that circumferential strains were induced chemically rather than mechanically) while also including the option for the investigator to superimpose longitudinal strain.

Recently several models have attempted to simulate an arterial-like flow environment by imposing aortic pressure waves or controlled flow rates onto an endothelialized tubular model. [69] Theses models inherently contain a combination of stimuli that are interdependent (e.g. flow, pressure, strain), which influences the input or response of other stimuli. Although these models incorporate similar flow characteristics encountered by an intact vessel, which may be important in endothelial response, a shear stress flow model

provides a more exact relationship between a well-defined biomechanical force and a measurable biological response without the influence of a deformable substrate. There are two main systems that are used to isolate the effects fluid shear stress; these are the parallel plate and cone and plate systems.

Parallel Plate System

The parallel plate flow chamber, in which a pressure differential is created between two slit (manifold) openings at either end of a rectangular chamber, causes uniform laminar flow to develop across the culture surface. Various sizes and aspect ratios have been used. [27, 70] Mechanisms used to create the pressure drop have included both gravity heads and active pumps. The parallel plate approach holds many practical attractions, including homogeneity of the stress stimulus, simplicity of the equipment, ease of medium sampling and exchange, ease of access to the culture (both physically and for microscope visualization) and small volumetric fluid requirement.

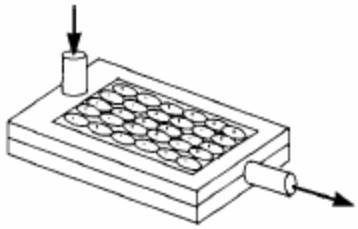

Figure 5. Diagram of a parallel plate flow chamber (diagram from Blackman, 2000).

A special version of the parallel plate device, incorporating a separate "settling chamber" and a curvilinear tapered inlet (based on boundary layer theory) has been devised

by Ruel et. al. [71] to optimize temporal and spatial flow field development in pulsatile stimulus situations. Tardy et al [72] augmented a conventional parallel plate chamber by imposing a rectangular obstacle in order to observe endothelial monolayer culture responses to shear stress gradients.

Current *in vitro* models lack the ability to control or even to quantify the precise mechanical input stimulus, particularly the loading rate, over a large dynamic range. For example, the parallel plate flow chamber is capable of applying a wide range of shear stress magnitudes and onset rates. However, current system designs do not allow arbitrary and independent control of the shear stress magnitude and onset times over a continuous range since flow is commonly generated by a constant pressure head, syringe pump, or peristaltic pump.

Cone and Plate System

The second main configuration used to study effects of shear stress is the cone and plate system, in which the rotation is imposed about a cone axis oriented perpendicular to the surface of a flat plate. [73] Since both the local relative velocity and the separation between the cone and plate surfaces vary linearly with radial position, this configuration achieves spatially homogeneous fluid shear stress on both of the respective surfaces. Depending on the conic taper and the imposed angular velocity, a wide range of shear stresses can be achieved, extending even into the turbulent flow regime. [74] Also, the hardware lends itself well to temporal modulation of shear stress, within the constraint of flow field development transients.

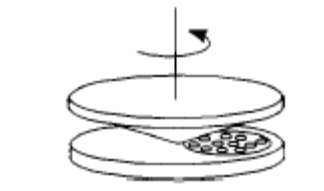

Figure 6. Diagram of a cone and plate shear device (diagram from Blackman, 2000).

The cone and plate shear system is identical in operation to the cone and plate viscometer and produces a shear stress distribution that is uniform throughout the fluid environment. This type of flow field is due to the cone's radial increase in gap height from the center of the plate surface, which compensates for linear velocity changes at different radial distances. [75] Fewell and Hellums [76] performed a detailed analysis of steady flow n the cone and plate viscometer and defined thresholds for the onset of significant secondary flow in terms of the cone angle and Reynolds number. [77] Reynolds number indicates the ratio, or relative importance, of the flow's inertial forces to its viscous forces. Large inertial forces, relative to the viscous ones, tend to favor turbulence, whereas large viscous forces stave off turbulence. Physical measurements in a cone and plate viscometer conducted by Sdougus et al [78] revealed that a modified Reynolds number (R), shown in equation 2, could be used to define three regimes of fluid behavior.

$$R = \frac{r^2 \omega \alpha^2}{12\upsilon} \qquad (2)$$

where r is the radius along the cone
ω is the rotational velocity
α is the cone angle
υ is the kinematic viscosity

With R< 1, a laminar flow environment is maintained with negligible secondary flows. For increasing values of R, secondary flows become more significant, and at R> 4, turbulence is induced. Also, the use of cones with greater angles and off-axis cones (i.e. tilted with respect to the axis of rotation) can be incorporated to create more complex flow fields such as turbulent and unsteady laminar flows that create simultaneous changes in temporal and spatial velocity profiles. [57]

Langille [79] was the first to demonstrate in a parallel rotating disk model (i.e. cone and plate shear system with a 0 deg cone angle) the application of an arterial-like waveform on the endothelium of dog aortic tissue. This model, which exposed the tissue to a linear spatial gradient in shear stress, investigated the influence of high levels of shear stress (up to 2000 dyn/cm^2) on endothelial injury, adhesion strength, and thrombogenic response. More recent models demonstrate the ability to deliver complex pulsatile flows. [80, 81]

Primary flow in the cone and plate geometry is expected to be in the azimuthal direction with a linear velocity profile from the stationary plate to the moving cone. Secondary flows in the vertical plane (radial flow direction) are expected to develop with increasing Reynolds number, as the flow changes from creeping flow to one in which the fluid's inertia is a key factor.

Many attempts have been made to investigate the flow between the cone and plate for small angles (angle << 1 deg). Fewell and Hellums 1977, [76] computed a numerical solution, while Sdougos et al. [78] studied the flow both analytically and experimentally.

New Shear System

In vivo, there are large temporal and spatial gradients of surface fluid shear stress near arterial branches. [30] The focal occurrence of atherosclerosis in such regions of disturbed flow [27] provides indirect evidence that fluid shear stress gradients may play a role in arterial wall pathology. Endothelial responses to shear stress have typically been studied *in vitro* under conditions where the time-average fluid shear stress is uniform. For this reason, we have chosen to develop a new device based on the cone and plate viscometer that delivers temporally varying levels of shear stress.

Blood flow patterns in large arteries (e.g. thoracic, abdominal, carotid, and brachial) share similar time-varying characteristics throughout the cardiac cycle. To develop an arterial-like shear stress waveform that would incorporate similar characteristics, we selected as a model a previously defined waveform by Dai, et. al. [60] This waveform encompasses several common temporal features found in large arteries (e.g. acceleration/deceleration rates, flow reversal, forward net flow).

Velocity waveforms generated by the combination controller/driver are implemented by a microstepping motor. Through software, the fluid dynamics can be programmed to simulate waveforms ranging from uniform laminar flows to more complex arterial waveforms. Precise control of the motor permits real-time or on-the-fly changes in acceleration and deceleration rates, velocity, and flow direction, which are key features in replicating arterial-type flows. The precision at which the programmed waveforms are replicated by the motor is ~0.02% (as reported by the manufacturer). Characteristics of this waveform include a peak shear stress of 43 dyn/cm^2 during systole, flow reversal during diastole to a maximum magnitude of -10 dyn/cm^2, and a frequency of 1.1 Hz. For the

measured waveforms, values of the angular velocity (rev/s) were measured directly from the motor and values of shear stress (dyn/cm^2) were computed at the plate surface.

CHAPTER 3

Results

Introduction

A variety of *in vitro* systems for applying mechanical loads to cell populations have been developed to gain insight into these mechanisms. However, limitations in the ability to precisely control relevant aspects of the mechanical stimuli have obscured the physical relationships between mechanical loading and the biochemical signals that mediate the cellular response. In an effort to better approximate the actual wall shear stresses experienced by ECs in arterial geometries *in vivo*, and to understand how these stimuli affect endothelial phenotype, we have designed and developed a cone and plate flow system to deliver shear stresses in arterial-like waveforms that mimic characteristics of flow in atheroprone and atheroprotected regions of the human carotid arteries. Validation of flow characteristics in the cone and plate system was done using Computational fluid dynamics (CFD) modeling and laser Doppler velocimetry (LDV). To validate the application of the device as a viable *in vitro* tool, the responses of ECs to arterial-like shear stress stimulus was evaluated in terms of cell morphology and regulation of protein expression.

Current Cone and Plate Shear System

Our lab currently utilizes a cone and plate system to simulate *in vivo* blood flow on confluent MAEC monolayers. The design is based on a cone and plate viscometer, in which a conical surface rotates relative to a stationary flat plate. The fluid medium between these surfaces is set in motion by the rotation of the cone, creating a uniform level of shear stress

throughout the fluid and therefore over the surface of the cells cultured on the plate. An essential feature of this geometry is the fabrication of a 0.5 deg cone angle with a smooth surface finish (i.e. free of defects). We use a cone constructed of Teflon with a 0.5 deg angle as shown in Figures 7 and 8.

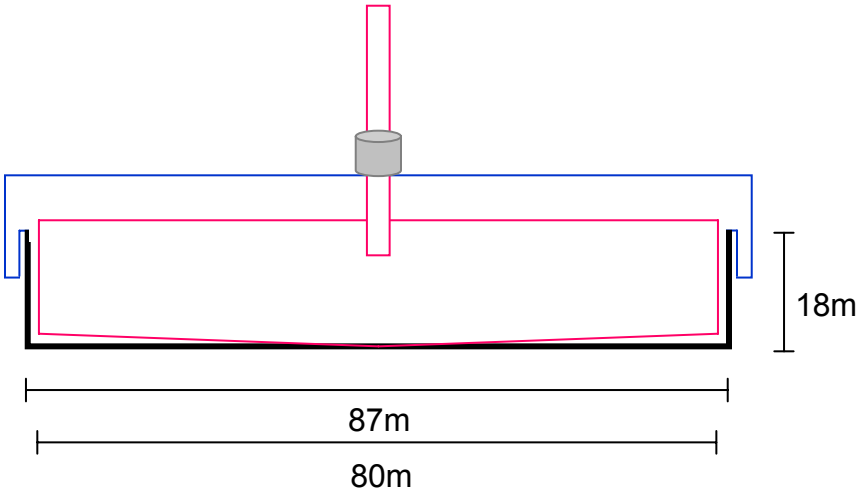

Figure 7. Teflon cone inside tissue culture dish.

Using a four-position magnetic stir plate, cones are continuously rotated to generate a shear stress of 15 dyn/cm^2, which simulates laminar shear (LS) conditions in the body. In order to simulate blood flow in regions of disturbed and oscillating shear (OS) we utilize a stepper motor (Japan Servo Motor) and a computer program (DC Motor Company, Atlanta, GA) which rotates the cone back and forth in order to generate ±5 dyn/cm^2 shear at a frequency of 1 Hz. All shear experiments are conducted inside a humidified incubator (37 deg C, 5% CO_2) and static controls are also maintained in the same incubators.

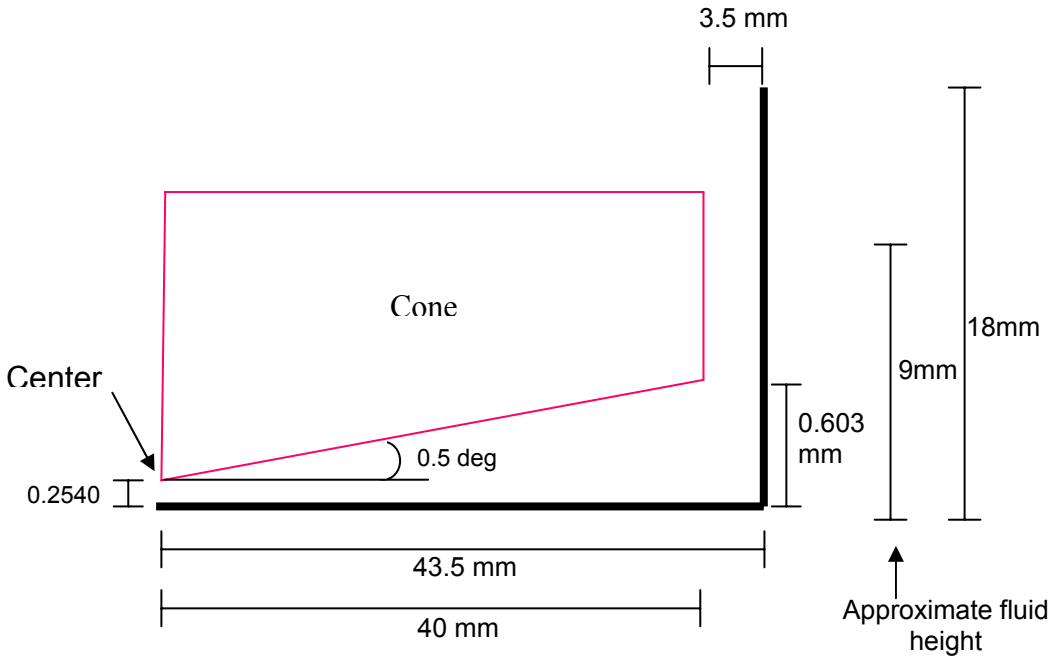

Figure 8. Cross-section of cone in tissue culture dish, shown from center of cone.

New Cone and Plate Shear System

We have developed a new controlled cell-shearing device based on the principles of a cone and plate viscometer but utilizing microstepper motor technology to independently control the dynamic and steady components of the hydrodynamic shear stress environment. The device was developed to impose controllable, quantifiable, and reproducible mechanical stimulation in the form of flow-induced shear stress on cells *in vitro*.

Control of the dynamic fluid environment was accomplished with a novel stepper motor drive system. The system is comprised of three major components: the microstepper motor, controller/indexer (OEMZL6104), and the interface software (Motion Architect, Parker Hannifin Corporation, Compumotor Division, Rohnert Park, CA). User-defined motor

parameters, including the acceleration, deceleration, angular velocity, duration, and direction, are programmed into the software to provide arbitrary definition of the exact mechanical stimulation over a wide range of conditions. This system was designed to produce shear stresses ranging up to 45 dyn/cm^2. The accuracy of the angular velocity of the motor is rated at ±0.02% of the maximum speed and the step resolution of the stator (i.e. motor's shaft) is 25,000 steps per revolution (or 0.0144 deg/step). Motor behavior was verified by checking output velocities versus input functions with the use of a tachometer (Check-line CDT-2000HD) aimed at the motor's shaft. Close correlation between the two was seen, with a maximum deviation of 0.5 RPM.

Shear stress profiles in both atheroprone and atheroprotected regions of the human carotid arteries published by Dai et. al. [82] were used to construct the motion profiles for this shear system (see Figure 9). Eight to ten significant points along a single cardiac cycle waveform were chosen upon which to base the program.

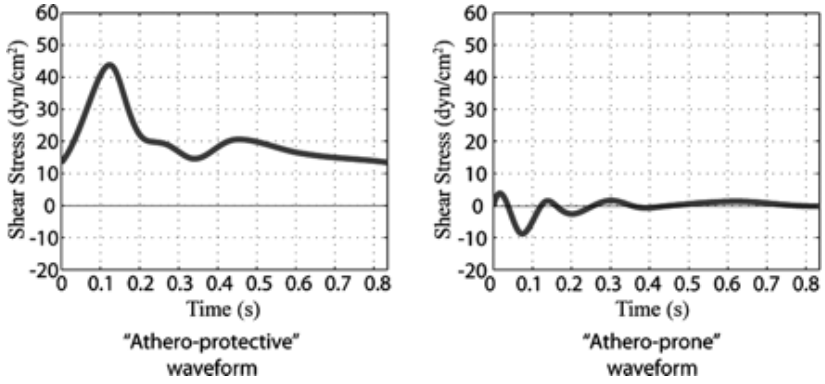

Figure 9. Shear stress waveforms published by Dai, et. al. [82]

Appropriate angular velocities corresponding to the desired shear stress values at these points were calculated using the relation:

$$\tau = \mu\omega\left(\frac{r}{h + r\alpha}\right) \tag{3}$$

where τ is wall shear stress
μ is fluid viscosity
r is radius
h is gap height
α is cone angle

modified from Newton's equations (eq 1, Chapter 1) to account for a non-zero gap height. Representative data that demonstrate the relation between wall shear stress and cone radius (see Figure 10) and angular velocity, respectively, are included in the appendix in Tables A and B. The angular velocity we chose (see Figures 11 and 12) will generate the desired shear stress at a radius of 30 mm. This corresponds to 48% of the plate surface area being exposed to shear values below the stated value and 52% above the stated value, as described in the cone and plate section of Chapter 2. Acceleration between these points was calculated linearly based on the change in velocity over the given time period.

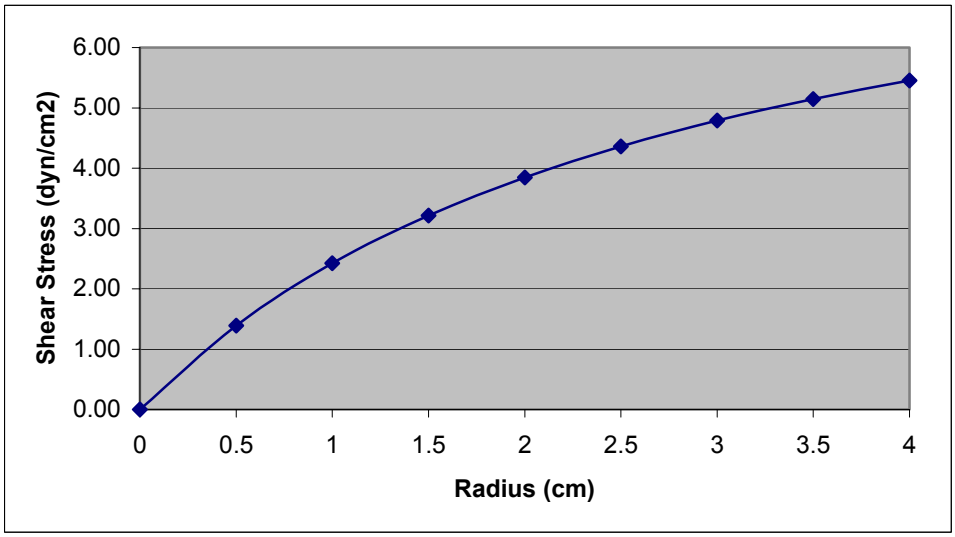

Figure 10. Calculated shear stress values for constant rotation at 100 RPM.

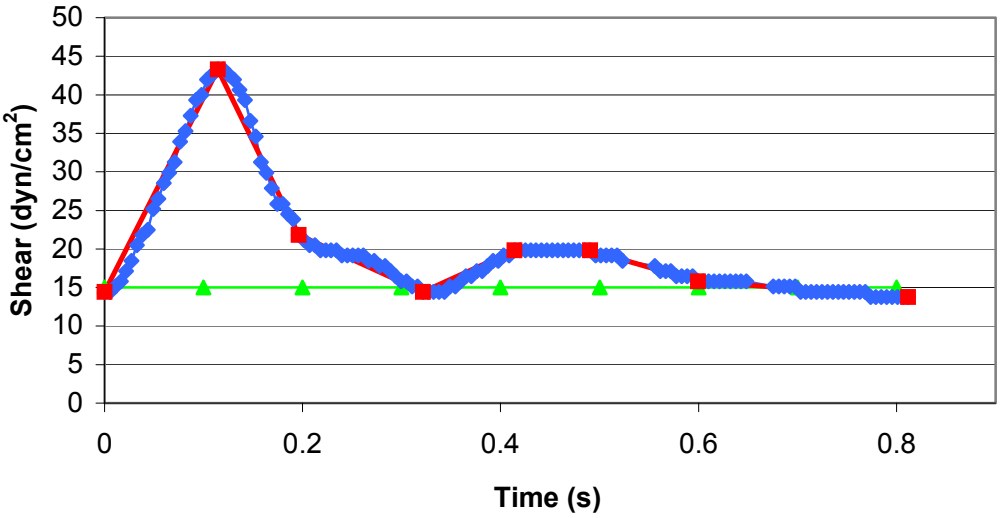

Figure 11. Atheroprotective program shear waveform. The blue trace is shear waveform published by Dai, et. al., [82] the red trace is shear waveform programmed in our new shear system, and the green trace is the shear stress value generated by our old shear system.

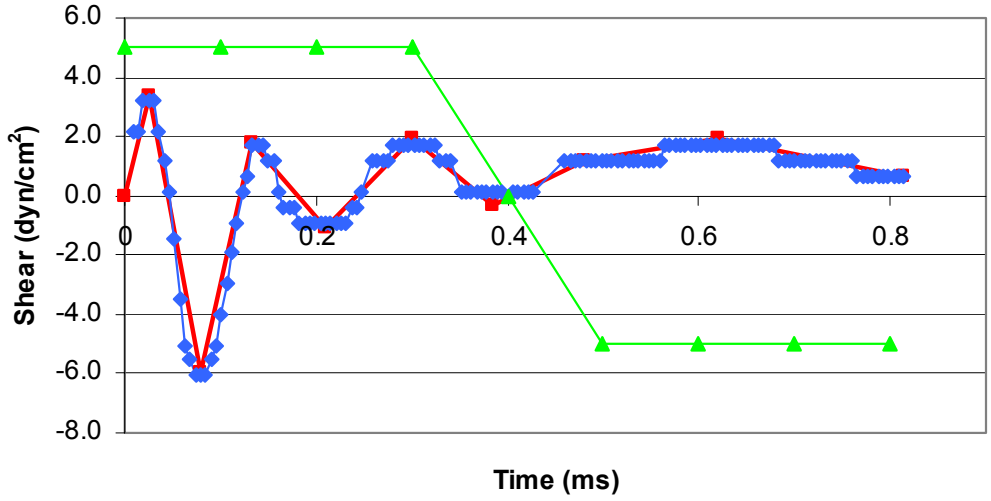

Figure 12. Atheroprone program shear waveform. The blue trace is shear waveform published by Dai, et. al., [82] the red trace is shear waveform programmed in our new shear system, and the green trace is the shear stress value generated by our old shear system.

These values (velocity, acceleration, time period, direction) were then used to write the code in the motor rotation program. The atherogenic motion program was designed to generate the desired shear stress values with a kinematic viscosity of 0.77 cSt (viscosity of DMEM with 10% FBS). The atheroprotective motion program was designed for a media viscosity of 1.40 cSt (viscosity of DMEM with 10% FBS and 5% Dextran-70 by volume). Dextran concentrations of up to 10 wt% in culture medium were found, by experiment to be compatible with the growth of endothelial cultures. [46, 83] This was done to decrease the necessary angular velocity and to help maintain laminar flow while still achieving the desired shear stresses. Maximum modified Reynolds numbers (as described in the cone and plate section of Chapter 2) generated by the atherogenic and atheroprotective motion programs are 0.24 and 0.35, respectively. These numbers correspond with flow in the laminar regime. The shear stress profiles generated by our motion programs show very good correlation with the waveforms developed from *in vivo* data, published by Dai et. al. [82]

Cellular Experiments

Cell Culture - Murine aortic endothelial cells (MAEC) were cultured in gelatin-coated 100 mm (87 mm actual inner diameter) tissue culture dishes with growth medium (Dulbecco's minimum Eagle's medium (DMEM with high-glucose and glutamax) containing 10% FBS (Atlanta Biologicals), 2.5 units/ml heparin, 1.7% ECGS (from bovine brain extract), and 1.1% MNEAA) as described by us. [84] For all experiments cells were used at passages 8-12 and maintained in incubators at 37 deg C and 5% CO_2.

Shear Experiments - Cells were grown to confluent monolayers and then were exposed to shear or static conditions for 24 hours. [85, 86] All cells were sheared using the

modified cone and plate viscometer as described previously in this chapter with either the current laminar shear (LS) or oscillatory shear (OS) systems or the new atheroprotective (AP) or atherogenic (AG) motion programs. Following shear exposure, cell morphology was determined by light microscopy.

Endothelial shape change *in vitro*, as well as established cell morphologies *in vivo*, prove to be faithful correlations of the nature of the applied fluid shear stress. [11, 55, 87, 88] After 24 hours, MAECs exposed to steady laminar shear will reorient from a static monolayer with cobblestone morphology to a well-characterized morphology in which the cells are elongated and aligned with the direction of flow. Maximum cell elongation is reached between 18 and 24 hours. [89] However, cells exposed to oscillatory shear maintain their cobblestone appearance., as shown in Figure 30.

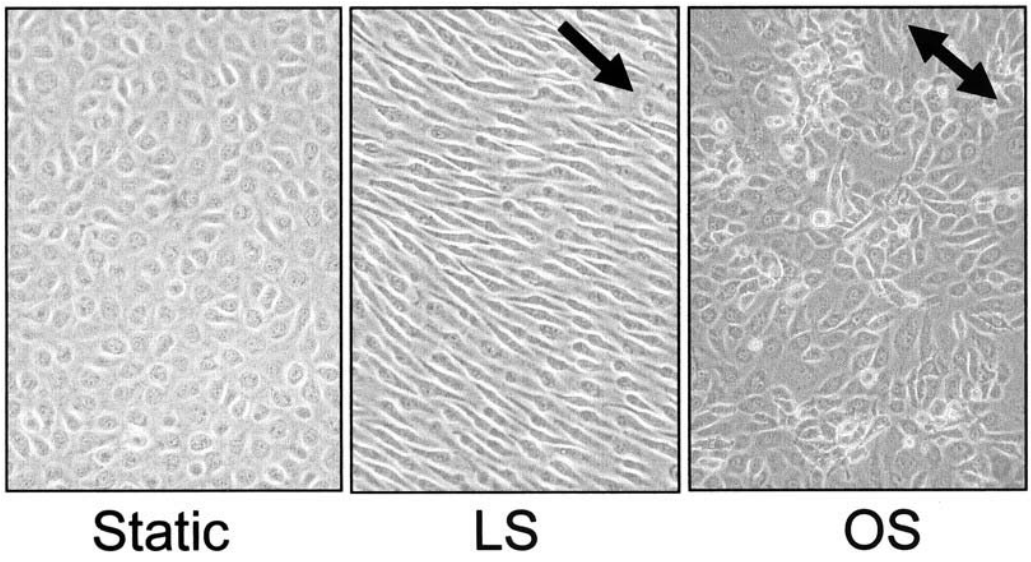

Figure 13. Confluent endothelial cells maintained in static conditions or sheared for 24 hours with unidirectional laminar shear (LS) (15 dyn/cm^2) or oscillatory shear (OS) (± 5dyn/cm^2, 1 Hz cycle). Arrows indicate the direction of flow.

To test the new AP and AG shear profiles, characteristic morphologies of MAEC monolayers exposed to these profiles for 24 hours were observed. Cells exposed to these

new physiologically representative flow conditions demonstrated morphologic behaviors consistent with those seen *in vivo* and with previous *in vitro* shear systems. Cells exposed to the AP shear waveform elongated and aligned in the direction of the flow while cells exposed to the AG shear waveform maintained a cobblestone morphology, as shown in Figure 14.

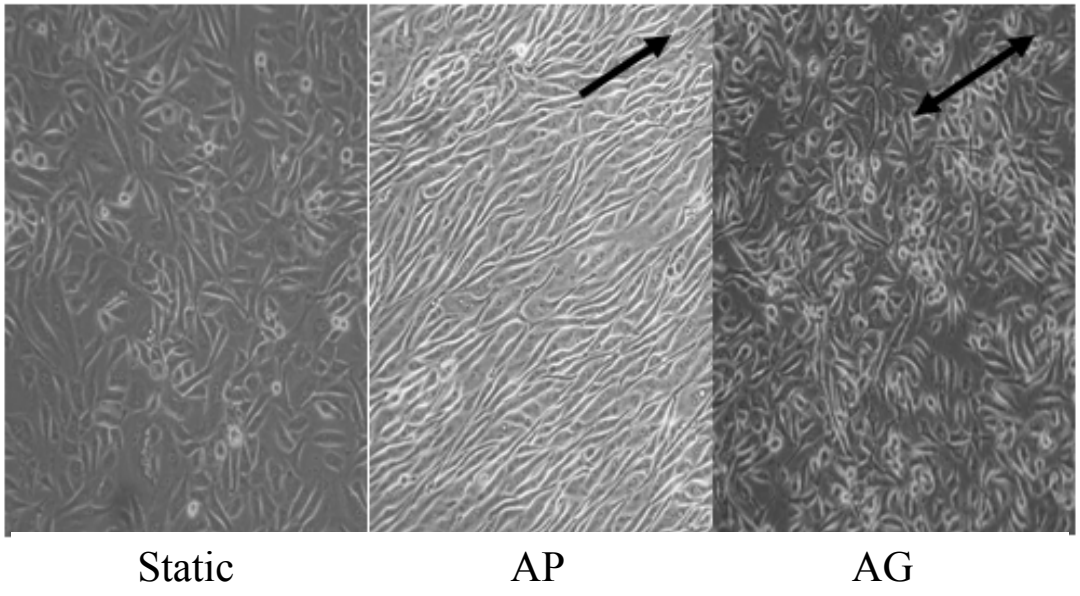

Figure 14. Confluent endothelial cells maintained in static conditions or sheared for 24 hours with the atheroprotective shear waveform (AP) or atherogenic shear waveform (AG). Arrows indicate the direction of flow.

Based on calculations, we know that the shear stress increases from the center of the plate outward. We studied the morphology of the cells at various radial distances and found that cells inside a 20 mm radius did not align. Cells located inside a radius of 20 mm experienced shear values increasing from 0 to 10 dyn/cm^2. This finding is consistent with published data that state the threshold level for cell alignment with uniform shear stress to be 8 dynes/cm^2. [11] Starting at a radius of 20 mm and moving outward, cells showed increasing alignment.

This was observed with both the current LS and new AP shear profiles, as shown in Figures 15 and 16, respectively.

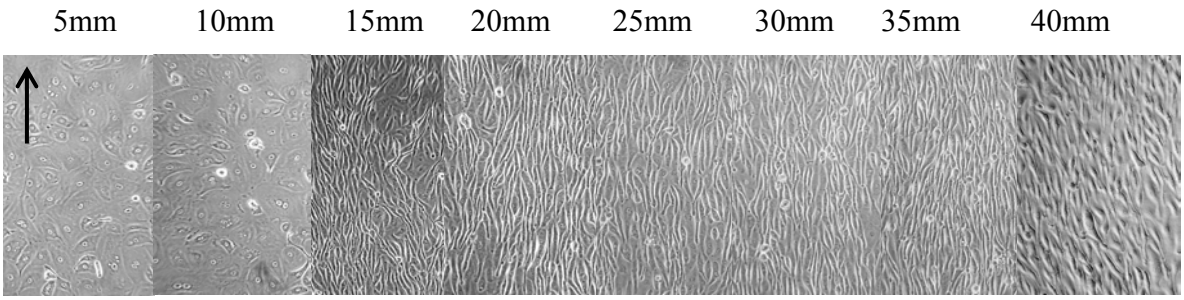

Figure 15. Pictures along radius from unidirectional laminar shear apparatus (arrow indicates direction of flow).

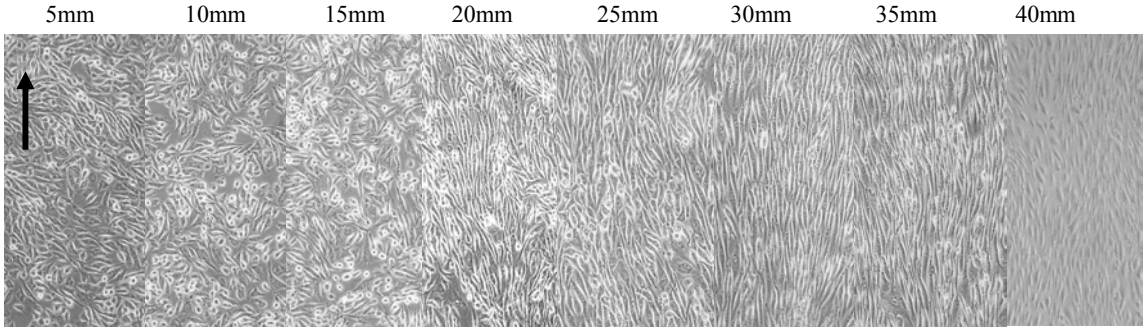

Figure 16. Pictures along radius from atheroprotective shear apparatus (arrow indicates direction of flow).

Preparation of Cell Lysates - Following shear exposure, MAEC were washed in ice-cold phosphate-buffered saline (PBS) and lysed in 0.6 ml of Ripa lysis buffer (5% 1M Tris (pH 8.0), 3% 5M NaCl, 5% DOC, 1% SDS, and 1% NP-40), supplemented with 0.01%, 0.1M PMSF protease inhibitor. Cell lysates were homogenized by sonication before protein content of each sample was measured using a Bio-Rad DC assay. [84]

Immunoblotting - Aliquots of cell lysates (20 μg of protein each) were resolved on a 10% SDS-PAGE gel and transferred to a polyvinylidene difluoride membrane (Millipore). [84] The membrane was incubated with a primary antibody overnight at 4 °C, and then with a secondary antibody conjugated with alkaline phosphatases (1 h at room temperature), which were detected by a chemiluminescence method. [84] The intensities of immunoreactive bands in Western blots were analyzed by using the National Institutes of Health IMAGE program. The following primary antibodies were used: polyclonal antibody for eNOS-S^{1177} (pS-eNOS) [Cell Signaling Technology, in rabbit, 1:1000 dilution], polyclonal antibody for total eNOS [Transduction Laboratories, in rabbit, 1:1000 dilution], BMP-4 [Santa Cruz Biotechnologies, mouse, 1:1000 dilution], pAKT-T308 [Cell Signaling Technology, 1:1000], tAKT [Cell Signaling Technology, 1:1000]. Actin [Santa Cruz Biotechnologies, goat, 1:1000 dilution].

Endothelial cell production of NO has been shown to be highly responsive to the flow environment *in vitro* and *in vivo*, reflecting immediate changes in enzymatic activity and short and long-term increases in endothelial nitric oxide synthase (eNOS) expression at both the mRNA and protein levels. [90-93] It has been shown that phosphorylated endothelial nitric oxide synthase (p-eNOS) is upregulated with laminar shear with respect to oscillatory shear. [94-96] To examine the regulation of eNOS activation by our new motion profiles, we measured changes in protein expression in MAECs after exposure to 24 hours of either AG or AP shear. As expected, P-eNOS was upregulated by the AP shear profile over the AG shear profile. Western blot results are shown in Figure 17 with quantification of the blot displayed in Figure 18.

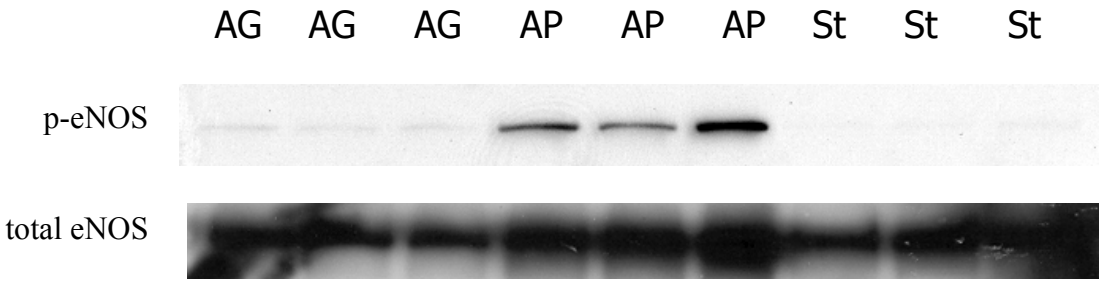

Figure 17. Western blot for eNOS. Protein samples from confluent MAEC monolayers exposed to the atheroprotective shear waveform (AP), atherogenic shear waveform (AG), or maintained at static (St) conditions for 24 hours.

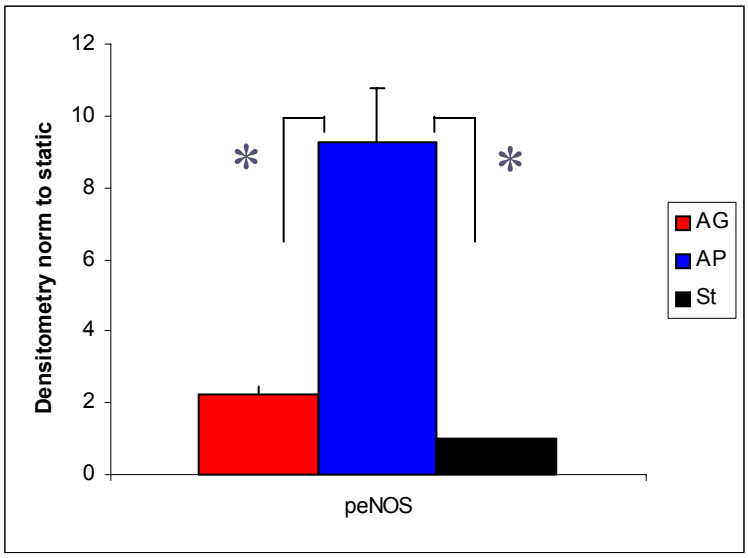

Figure 18. Numerical analysis of p-eNOS western blot. p-eNOS values were normalized to total eNOS. Protein samples from confluent MAEC monolayers exposed to the atheroprotective shear waveform (AP), atherogenic shear waveform (AG), or maintained at static (St) conditions for 24 hours. (n=3, *: $p<0.05$)

Bone morphogenic protein-4 (BMP-4) is a pro-inflammatory, and hence atherogenic, molecule that is upregulated in oscillatory flow regions of the vasculature. Cells exposed to oscillatory shear exhibited an upregulation of BMP-4 (both immature and mature forms) versus cells exposed to unidirectional laminar shear. [97, 98] To examine the regulation of BMP-4 expression by our new motion profiles, we measured changes in protein expression in MAECs after exposure to 24 hours of either AG or AP shear. As predicted, BMP-4 was upregulated by the AG shear profile over the AP shear profile, see Figures 19-21.

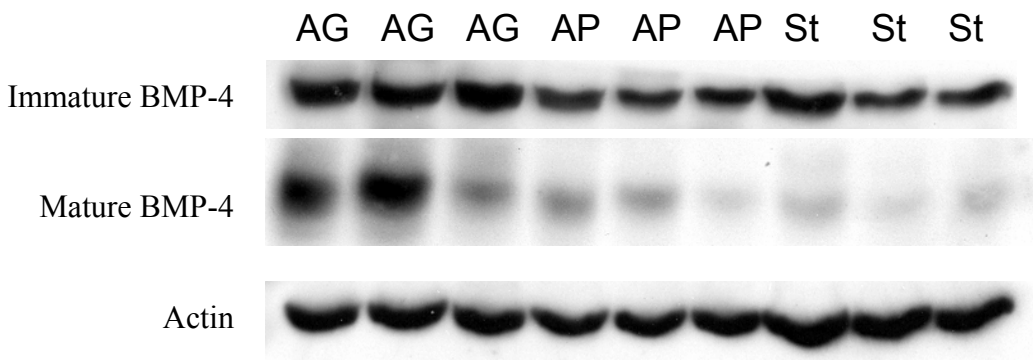

Figure 19. Western blot for BMP-4. Protein samples from confluent MAEC monolayers exposed to the atheroprotective shear waveform (AP), atherogenic shear waveform (AG), or maintained at static (St) conditions for 24 hours.

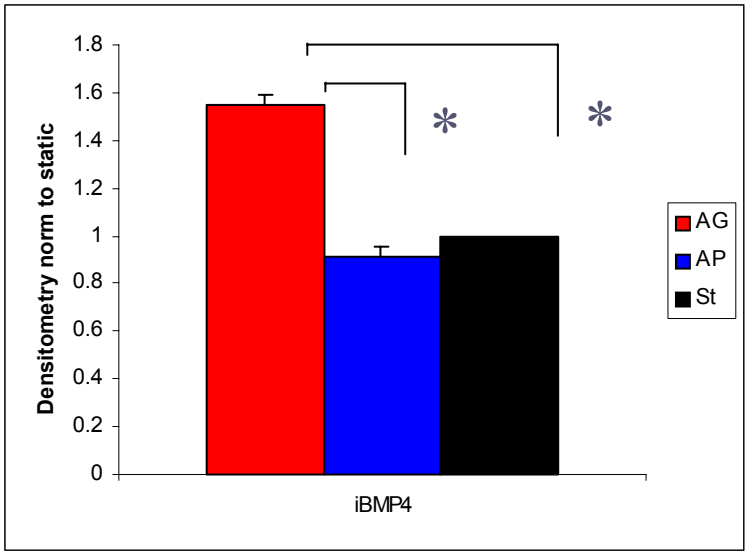

Figure 20. Numerical analysis of immature BMP-4 western blot. The immature form of BMP-4 (i BMP4) was normalized to actin protein levels. Protein samples from confluent MAEC monolayers exposed to the atheroprotective shear waveform (AP), atherogenic shear waveform (AG), or maintained at static (ST) conditions for 24 hours. (n=3, *: p<0.05)

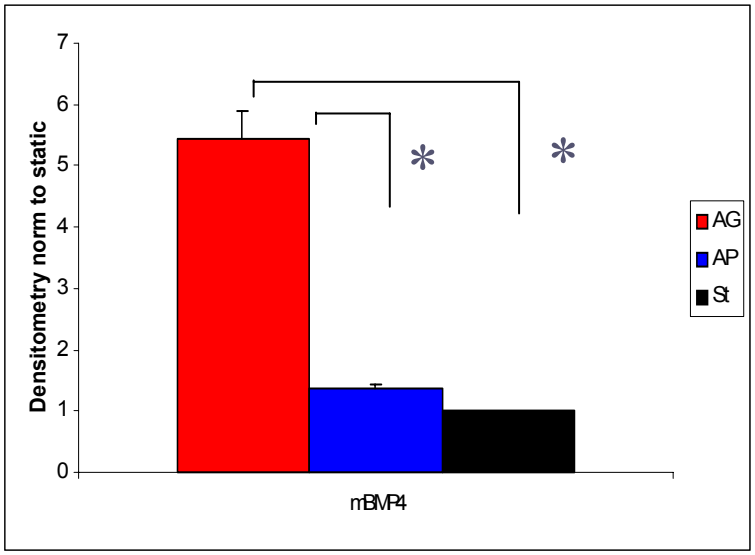

Figure 21. Numerical analysis of mature BMP-4 western blot. The mature form of BMP-4 (mBMP4) was normalized to actin protein levels. Protein samples from confluent MAEC monolayers exposed to the atheroprotective shear waveform (AP), atherogenic shear waveform (AG), or maintained at static (St) conditions for 24 hours. (n=3, *: p<0.05)

We present experimental results demonstrating the functional and structural responses of endothelial cell cultures to dynamically applied shear stress. The controlled cell shearing device is a novel tool for elucidating mechanisms by which mechanical forces give rise to the biological signals that modulate cellular morphology and metabolism. To validate the fluid mechanics of this system and demonstrate the dominance of viscous forces under steady and arterial flow, we performed CFD modeling and LDV.

Computational Fluid Dynamics (CFD) Modeling

In order to correlate calculated rotational velocities with the associated development of the shear stress at the plate surface, CFD software was used to solve for the three-dimensional (3D) axisymmetric cone and plate geometry. With CFD, the computer calculates the parameters of interest (i.e. velocity and pressure) for each grid point. The computational grid (mesh) discretizes the problem in space. Calculations are carried out at regular intervals to simulate the passage of time, so the solution is also temporally discrete. More grid points means less volume between points of calculation, which means simulation is more accurate and realistic. We first used CFD to verify that the calculated rotational velocities were in fact generating the desired shear stress levels. We then investigated the acceleration, deceleration, and rotational velocities used in the AP and AG motion programs to determine the significance of secondary flow.

The cross-sectional geometry and mesh of the fluid environment between the cone and plate surfaces were constructed using CFD-Ace software. The boundary condition (BC) at the plate surface of the mesh was modeled as a stationary, fixed surface (v=0), while the cone surface was modeled as a fixed, rotating surface. The boundary at the cone center was

defined with an axisymmetric condition. The outer edge of the fluid volume was investigated using four different boundary conditions, as describe below.

Boundary Condition 1

The outer boundary was set at the edge of the cone (r=40mm) and was modeled as a fixed, stationary surface.

Figure 22. CFD mesh for boundary condition 1.

Boundary Condition 2

The outer boundary was set at the edge of the cone (r=40mm) and was modeled as a free surface, with a constant pressure condition.

Figure 23. CFD mesh for boundary condition 2.

Boundary Condition 3

The outer boundary was formed by the edge of the dish (r=43.5mm) and the upper surface of the fluid between the outer edge of the cone and the wall of the dish was modeled as a fixed, stationary surface.

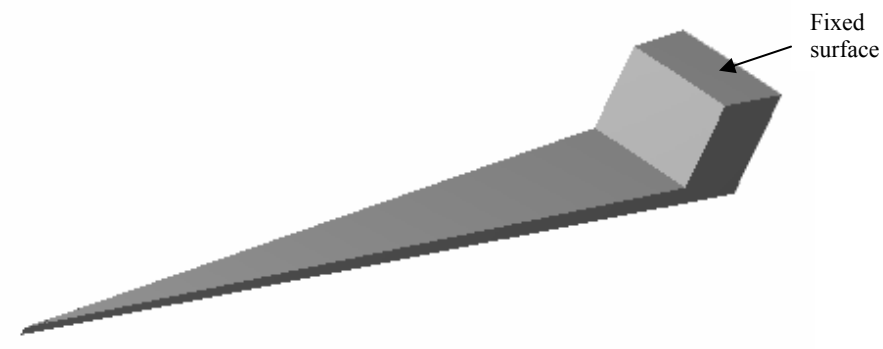

Figure 24. CFD mesh for boundary condition 3.

Boundary Condition 4

The outer boundary was formed by the edge of the dish (r=43.5mm) and the upper surface of the fluid between the outer edge of the cone and the wall of the dish was modeled as a free surface, with a constant pressure condition.

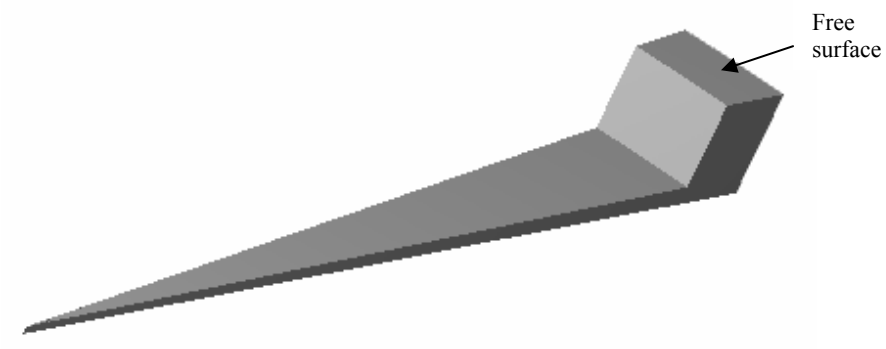

Figure 25. CFD mesh for boundary condition 4.

The mesh object was and numeriacally solved using CFD-Ace Software by employing the 3D, time-dependent Navier-Stokes equations for the circumferential shear stress. All shear stresses were calculated at a distance of 1-2 μm above the plate surface.

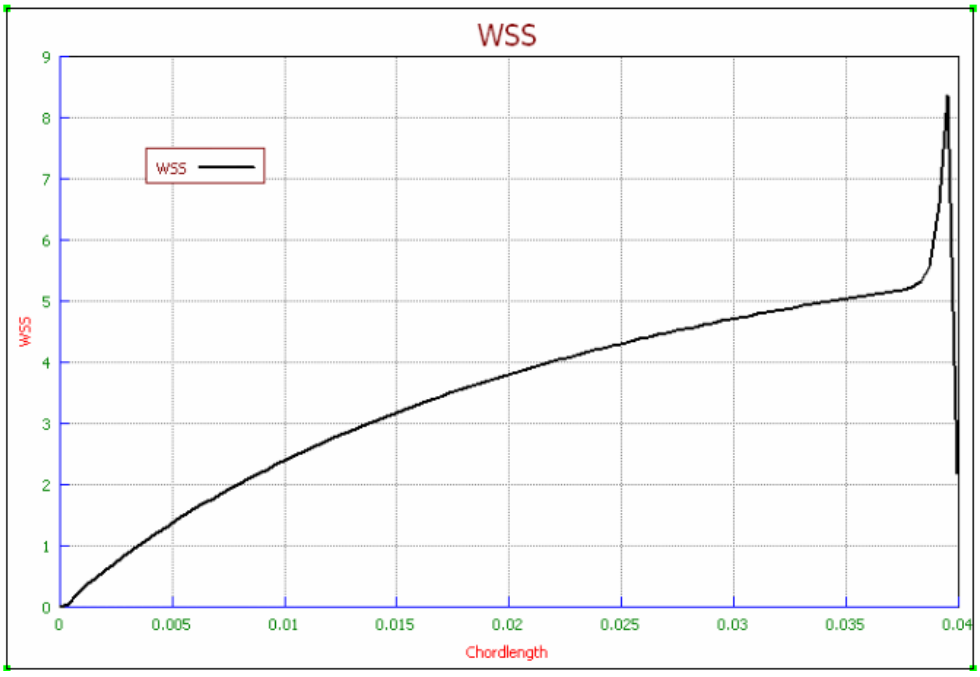

Figure 26. Wall shear stress (WSS) in dyn/cm^2 vs. plate radius (Chordlength) in cm, using boundary condition #1. Simulation was run at constant cone rotation of 100 RPM.

Using BC 1, calculations showed a steady increase in shear stress along the plate radius with a large spike in shear stress at the outer edge of the cone (starting at radius ≈35 mm) (see Figure 26). This is mostly likely due to the imposed boundary conditions, and is not an actual effect of the flow. To test this, we modified the boundary condition, changing it from a fixed surface to a free surface.

Using BC 2, the shear stress showed a steady increase along the radius and continued to increase along the same curve out to the edge of the cone. The spike in shear stress generated by the simulation using BC 1 was no longer present (see Figure 27).

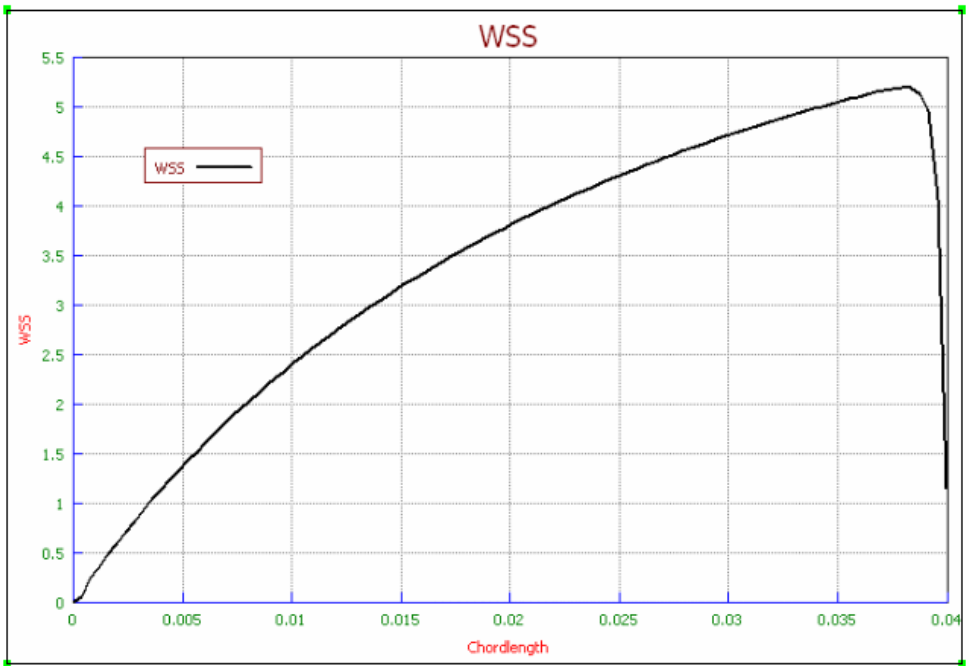

Figure 27. Wall shear stress (WSS) in dyn/cm^2 vs. plate radius (Chordlength) in cm, using boundary condition #2. Simulation was run at constant cone rotation of 100 RPM.

With BC 3, the shear stress along the plate followed the same curve as it did with BC 2. The difference in this simulation is that we included the fluid between the outer edge of the cone and the wall of the dish (see Figure 28). This additional volume did not affect the magnitude of the shear between the cone and the bottom surface of the plate. We were able to visualize the flow circulation at the outer edge of the cone, which showed two vortices.

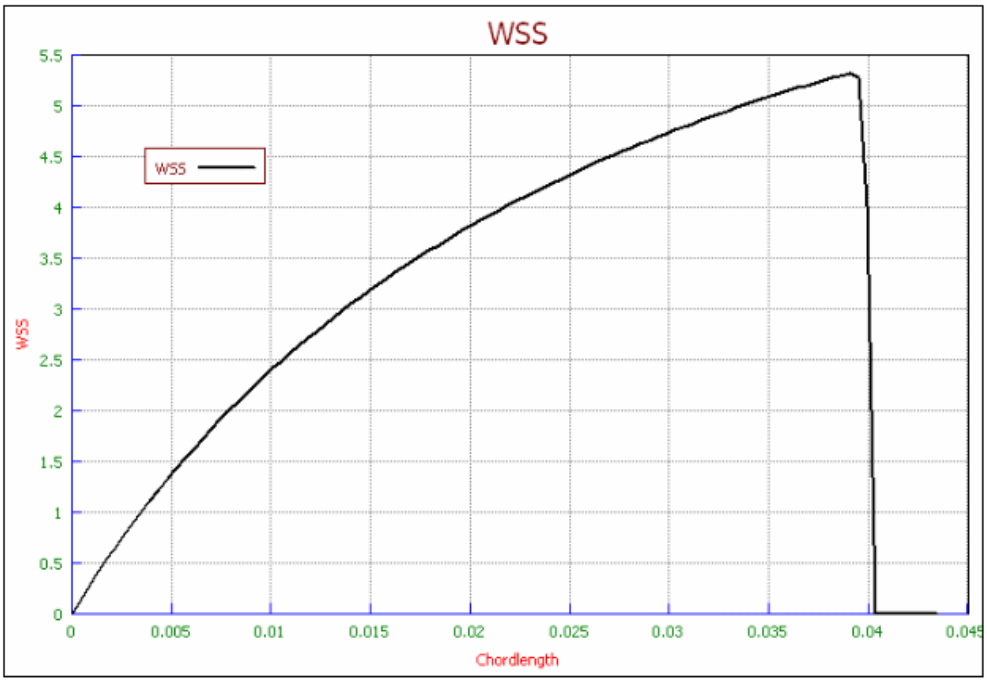

Figure 28. Wall shear stress (WSS) in dyn/cm^2 vs. plate radius (Chordlength) in cm, using boundary condition #3. Simulation was run at constant cone rotation of 100 RPM.

Calculations with BC 4 yielded the same shear stress profile as simulations with BCs 2 and 3, with the exception of a small spike in shear stress at the very edge of the cone (see Figure 29). Again, this is probably due to the imposed boundary conditions and does not happen in the actual fluid flow. The flow in the volume between the outer edge of the cone and the wall of the plate showed a single vortex under these conditions.

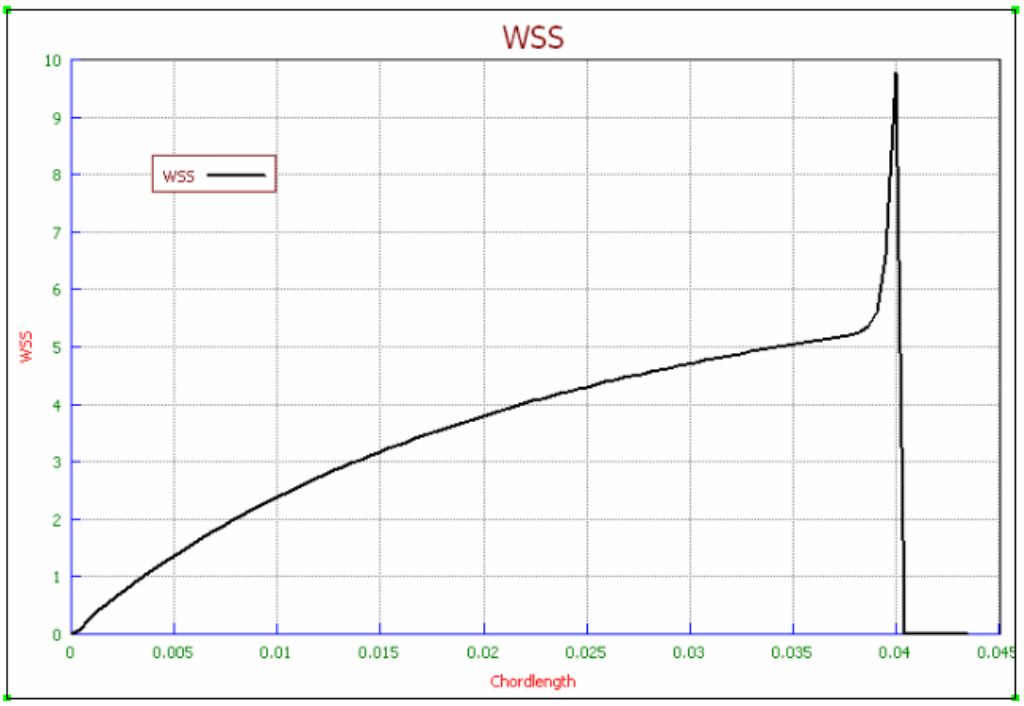

Figure 29. Wall shear stress (WSS) in dyn/cm^2 vs. plate radius (Chordlength) in cm, using boundary condition #4. Simulation was run at constant cone rotation of 100 RPM.

Laser Doppler Velocimetry (LDV)

The fluid velocity in the cone and plate system was measured using LDV. Laser Doppler velocimetry is a technique to measure flows using the Doppler effect. Two lasers, with the same wave length, but put in different directions, are used. As micron-sized solid particles entrained in a fluid pass through the intersection of two laser beams, the scattered light received from the particles fluctuates in intensity. The frequency of this fluctuation is equivalent to the Doppler shift between the incident and scattered light, and is thus proportional to the component of particle velocity, which lies in the plane of the two laser

beams and is perpendicular to their bisector. The velocity direction can be fixed if one of the laser beams has a frequency slightly different from that of the other.

The fluid used for the LDV experiments was a solution of saturated sodium iodide, glycerin, and deionized water in a volumetric ratio of 79:20:1. Although the viscosity of this solution (3.39 cSt) was higher than that of the media used in the shear experiments (0.77 cSt), the shear rate would be the same for both fluids. The shear stress can then be calculated by multiplying the shear rate by the viscosity (as discussed in Chapter 2). The refractive index of the fluid (1.49) matched that of the Plexiglas (polymethylmethacrylate) plate used to represent the tissue culture dish. Matching the refractive index of the solution minimized optical distortion of the laser beams used in these studies. Neutrally buoyant silicone particles (TSI, Inc., St. Paul, MN) were used in all of the LVD experiments to seed the flow. These particles had a mean diameter of 1.5 μm.

Light was generated by a 5 W, argon-ion laser plasma tube (Model 70 Innova, Coherent, Santa Clara, CA) and was subsequently passed through a fiber optic drive (Aerometrics, Sunnyvale, CA). It was divided into two separate wavelengths 488nm (blue) and 514.5nm (green). Frequency shifting was necessary and effective in experiments for measuring the velocity.

Velocity measurements were taken at 25μm increments vertically, from the plate surface to the cone surface. Measurements were taken in the radial direction at increments of 5mm from the center of the cone. Data gathered at a radius of 20mm is shown in Figure 30.

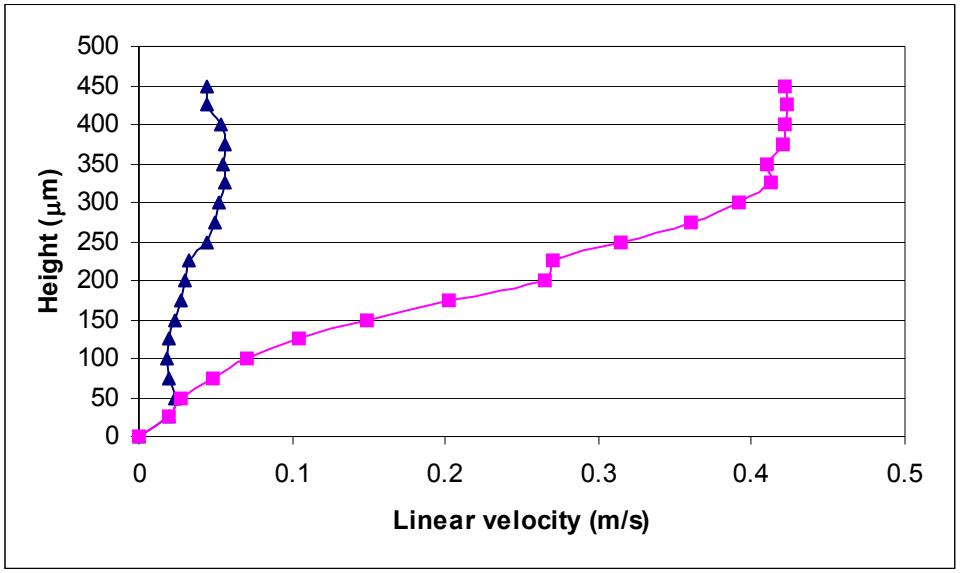

Figure 30. Velocity profile taken at radius=20mm, from plate surface (h=0) to cone surface (h=425mm). Cone rotation was constant at 100 RPM (corresponding linear velocity is 0.419 m/s. Tangential velocity is represented by cubes, radial velocity (secondary flow) is represented by triangles.

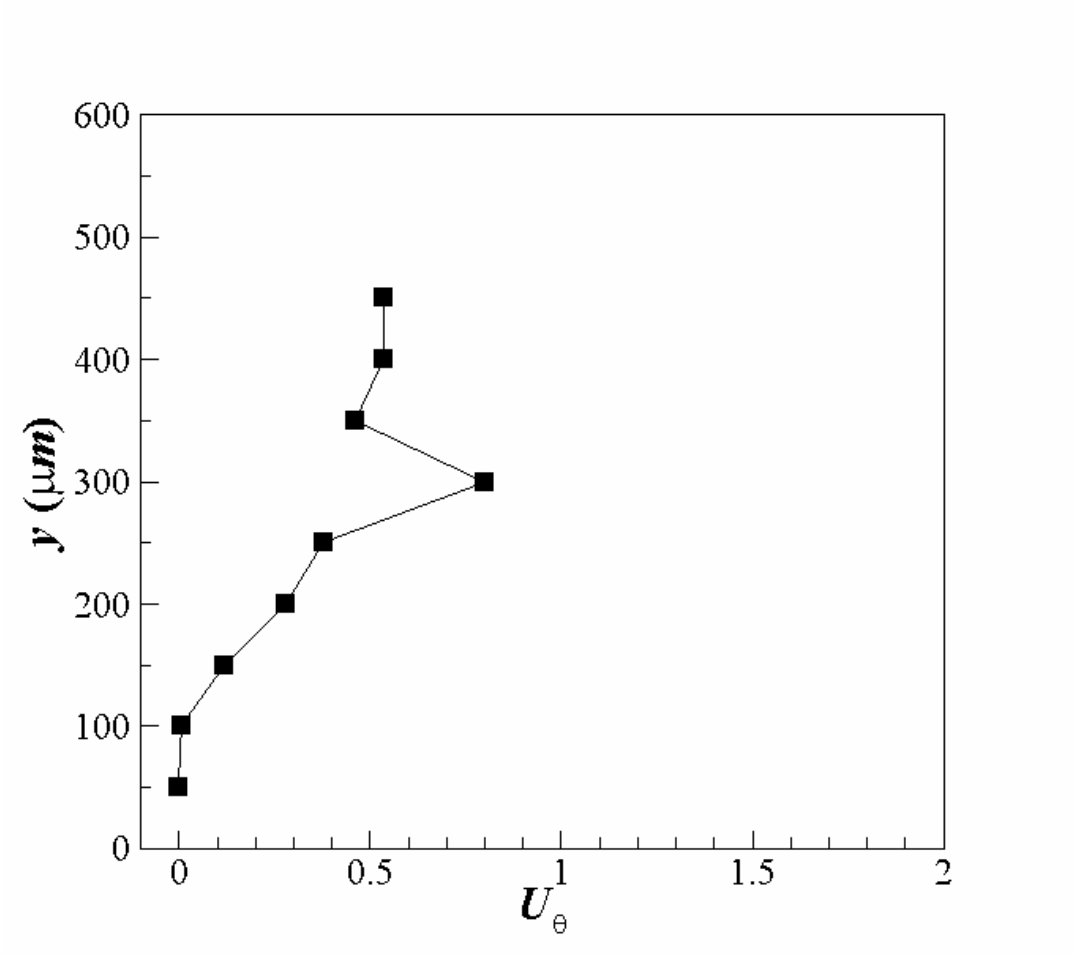

Figure 31. Velocity profile taken at radius=30mm, from plate surface (h=0) to cone surface (h=450mm). Cone rotation followed the AP shear waveform. This video demonstrates the rotational velocity over 0.81s (representative of 1 cardiac cycle).

CHAPTER 4

Discussion

Over the past twenty years, research has been aimed at modeling various flow conditions on endothelium *in vitro* in order to understand how biomechanical forces (i.e. shear stress) affect cellular responses. Although these studies have identified many flow responsive pathways, most have focused on modeling the flow environment with steady, sinusoidal, or turbulent flow conditions, [14] which do not possess the complex time-varying features of *in vivo* blood flow. [61] We described the development of an *in vitro* system to simulate the shear stress component of human blood flow waveforms on cultured endothelial cells. An arterial-like shear stress waveform developed by Dai et. al. from MRI and ultrasound data from human subjects [82] was modeled using a microstepping motor and controller. This device was tested by evaluating the biological responses of ECs to this new type of flow as well by using CFD and LDV to verify flow characteristics.

We have demonstrated a new device to study cellular responses to hydrodynamically applied shear stress. A microstepper motor control system was used to transform a traditional cone and plate viscometer into a cell-shearing device that can achieve maximum versatility and control of the mechanical input. Programming the acceleration, deceleration, velocity, duration, and direction of the motor permits precise and independent control of the shear stress magnitude and the rate of change of shear stress. By utilizing these features, the device can be used to investigate the response of cells to a wide range of shear regimes.

Arterial-like shear stress waveforms, published by Dai et.al., [60] were programmed into a controller/driver to control a microstepping motor. Values of shear stress from these

waveforms were used to calculate the appropriate angular velocity (rev/s) of the cone. These waveforms include several major characteristics, including a maximum shear stress of 43 dyn/cm^2 during peak systole, flow reversal during diastole that reaches –10 dyn/cm^2, time-average shear stress values of 20 dyn/cm^2 (AP waveform) and 0.5 dyn/cm^2 (AG waveform), and a frequency of 1.1 Hz. The biomechanical limits of these waveforms (i.e. maximum, minimum, and time-averaged amplitude of shear stress) agree well with published results of near wall shear stress computations in the abdominal aorta using MRI techniques, in which a maximum shear stress during systole ranged between 30 to 60 dyn/cm^2, minimum shear stress during flow reversal was -4 to -13 dyn/cm^2 and time-averaged shear stress ranged between 3 to 7 dyn/cm^2. [99, 100]

Validation of this design, particularly the conformity of the time-varying shear stress with respect to the programmed input, required evaluation of the unsteady flow associated with more complex, arterial like flow simulations. CFD software was used to investigate the development of the shear stress on the plate surface as a function of time, velocity, and radius. This device is capable of accurately applying time-varying shear stress to a population of cells for physiologic mechanotransduction experiments. The ability to precisely apply a range of shear stress gradients to endothelial cells will allow evaluation of the contribution of more temporally varying shear profiles, such as those seen *in vivo*. This technology can be used to expose endothelial cells to flow conditions that mimic those in distinct regions of the circulatory system (i.e. atheroprone or atheroprotected regions) to provide additional insight into pathologic conditions (e.g. atherogenesis) or phenotypic heterogeneity.

This system does not incorporate the additional stress components - hydrostatic pressure and hoop stress - encountered by the endothelium *in vivo*. However, in order to understand the relative contribution of the complex shear stress component of the arterial flows on EC response, we have developed this arterial shear stress model to provide a more exact relationship between a well-defined biomechanical force and a measurable biological response. We set out to fully characterize this new type of arterial-like waveform on the biological response of MAEC.

With the introduction of a new device, it is necessary to reproduce results obtained with the preceding technology. This device was designed for the purpose of investigating the effect of the unsteady or dynamic flow on endothelial cellular response in an effort to represent *in vivo* conditions more accurately than current time-averaged, steady shear systems. Endothelial morphology and orientation in arteries *in vivo* correlate with the local hemodynamic environment. [87, 88] Similar results have also been observed with steady and pulsatile shear stress patterns *in vitro*. [11, 101] We show ECs exposed to arterial-like flow for 24 hours change shape from a cobblestone morphology to one that is aligned with the direction of flow. This result is in agreement with several studies indicating that ECs elongate and align in the direction of flow when exposed to time-averaged, steady shear stress for a minimum of 18 hours. [55, 56] This response is also similar to ECs in straight, non-bifurcating arterial segments. [87] This finding does not hold for oscillatory flow with low shear values, where the shape of the cells remains relatively cobblestone appearance in comparison to an equivalent unidirectional, laminar shear stress stimulus, [38] thus indicating the importance of the direction and magnitude of the flow vector. Literature suggests that disturbed flow, as found near arterial branches, is a more likely agent than either high or low

shear in implicating the process of atherogenesis. Experiments in steady separated flow point strongly to fluid shear stress gradient as the common element in disturbed flow regions that trigger responses that may be important in the pathogenesis of atherosclerosis. [57] These findings further support the need for a device that generates temporally varying levels of shear stress.

In addition to cell morphology, we evaluated the regulation of protein expression by arterial shear stress levels *in vitro* and compared it to data obtained previously with using 15dyn/cm^2 unidirectional laminar shear or ±5 dyn/cm^2 oscillatory shear. One protein we studied was eNOS, which plays a critical role in maintaining the contractile, remodeling and hemostatic environment of arteries [102, 103] and has been shown to be highly responsive to flow *in vitro*. A significant increase in p-eNOS protein was observed for the AP shear profile after 24 hours, but not for the AG profile. Cells exposed to the AP shear profile had values that increased to numbers similar to those seen after exposure to unidirectional laminar shear (15 dyn/cm^2) for 24 hours, when compared to cells exposed to the AG shear profile or oscillatory shear (±5 dyn/cm^2), respectively.

Another protein we investigated was BMP-4, a pro-atherogenic protein that has been shown to increase in endothelial cells exposed to oscillating and low levels of shear stress. An increase in BMP-4 protein expression (both mature and immature forms) was observed for the AG shear profile after 24 hours, as compared to ECs exposed to the AP shear profile. Cells exposed to the AG shear profile had values that increased to numbers similar to those seen after exposure to oscillatory shear (±5 dyn/cm^2) after 24 hours.

The techniques of LDV and CFD analysis are complementary evaluation tools in research. Though CFD analysis can evaluate any physical quantity at any position, suitable mathematical models and correct boundary conditions should be carefully selected. LDV can assure high accuracy at the particle data points, though the observable region is restricted. The advantages of LDV are that unsteady phenomenon can be captured and that it provides experimental, as opposed to analytical data. The disadvantages are that the sections that can be studied are limited by the geometry and non-planar visualizations are impractical.

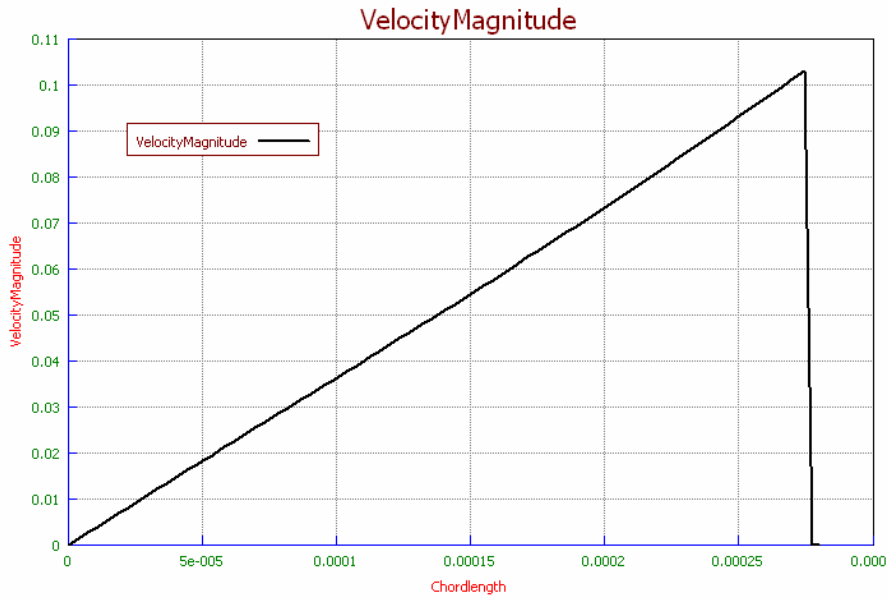

Figure 32. Velocity profile generated by CFD. Results are for velocity versus chordlength, at a radius of 2.5mm, angular velocity of 400 RPM. Chordlength is gap height (m) between plate surface (0) to cone surface (0.000275)

Comparison of velocity profile shapes calculated with CFD with those generated from experimental data gathered by LDV show good correlation, as shown in Figures 31 and 32. This confirms that the velocity of the fluid at the cone surface is in fact the same as that

of the cone and that the velocity profile is approximately linear with respect to gap height. The experimental deviation from a linear velocity profile, as predicted numerically by CFD, could be due to secondary flow along the radial axis or experimental artifacts such as errors in the adjustment of the probe volume height or a slight tilt in the axis of the cone. Overall, the LDV data are supportive of our device since we are primarily concerned with the fluid velocity near the plate surface, not with variations in flow within the entire fluid volume.

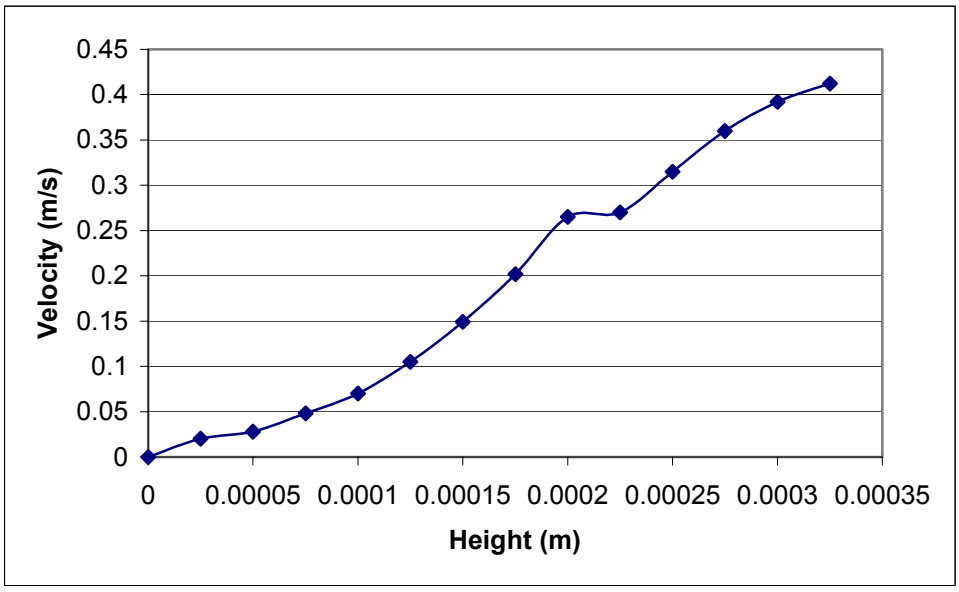

Figure 33. Velocity profile generated by LDV. Measurements taken at a radius of 20mm, angular velocity of 200 RPM. Height is distance between plate surface (0) and cone surface (0.000325).

The wall shear stress values calculated using Newton's equation, modified for our gap height, (see equation 3, Chapter 3) were very close to those generated by the CFD simulations, using all four boundary conditions (see Figures 33 and 34). With the exception of the region from the radius of 35mm to 40mm, the calculated shear values were all within 0.5 dyn/cm^2 of the CFD generated values. Outside the radius of 35mm, calculated values

deviated, sometimes significantly, from CFD generated values. This is most likely due to three reasons:

- The modified Newton's equation does not take into account secondary (radial) flow, which may become significant at larger radius values where edge effects become important.
- CFD modeling is highly sensitive to boundary conditions. The significant differences between calculated and CFD generated shear values were only apparent with 2 of the 4 boundary conditions. This means it is likely, at least in part, that the discrepancy is an artifact of the model.
- At the edge of the cone (r=40mm) a discontinuity is produced in the mesh used for the CFD computations. Accurate solutions are difficult to resolve at points of discontinuity, therefore it is not correct to assume values generated at these regions as factual, without further confirmation.

In addition to the velocity profile and wall shear stress, the modified Reynolds number was calculated to determine if the flow was within the laminar domain. Using equation 2 (Chapter 2) the maximum modified Reynolds number achieved with our system was determined to be 0.35 for the AP shear profile and 0.236 for the AG shear profile. These values were calculated at a cone radius of 40mm, where the modified Reynolds value would be highest. Since both of these numbers are significantly less than one (the condition that defines laminar flow in a cone and plate system) we can confidently state that the flow between the cone and plate surface remains laminar throughout the entire shear cycle.

Since there is such close correlation between the modified Newton's equation and CFD-generated shear stress values, it is really only necessary to use CFD to study the outer

edge of the cone (r > 30mm), where secondary flow may become important. Shear values within the well-defined region inside the cone radius of 30mm can be calculated by hand using Newton's equation.

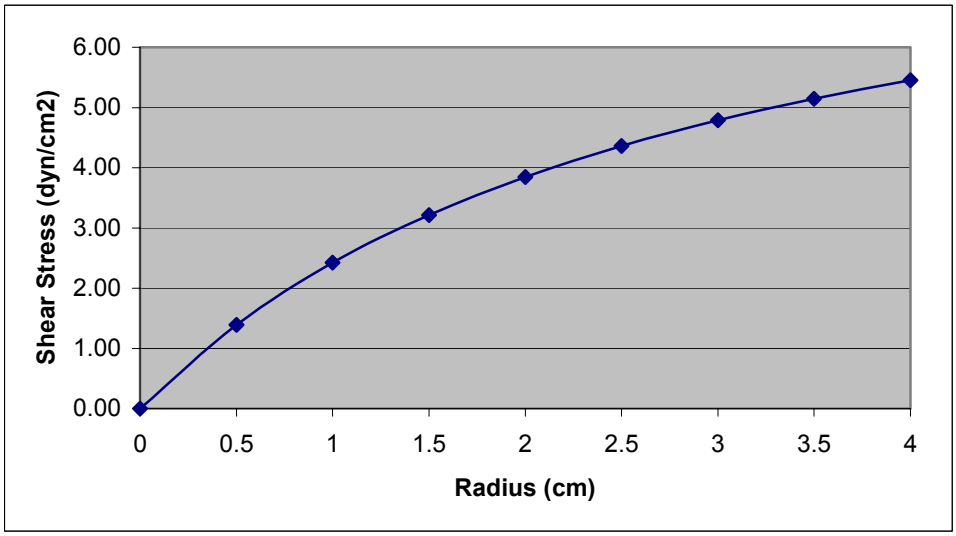

Figure 34. Calculated wall shear stress (WSS) in dyn/cm^2 vs. plate radius in cm at 100 RPM.

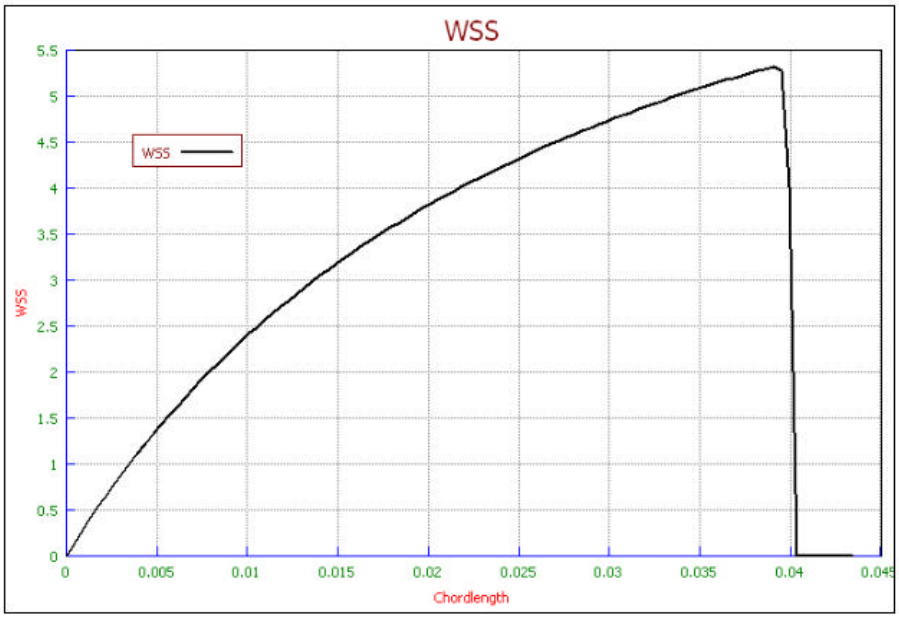

Figure 35. Wall shear stress (WSS) in dyn/cm^2 vs. plate radius (Chordlength) in cm, using boundary condition #3. Simulation was run at constant cone rotation of 100 RPM.

Analysis of the flow characteristics in this new cone and plate shear system revealed that the shear is not constant across the plate surface and that very quick changes in cone rotation speed generate a temporary deviation from a linear velocity gradient. This non-linear velocity gradient results in a decreased magnitude of wall shear stress at the plate surface. However, the fact that the wall shear stress may not be reaching the maximum values in the AP and AG waveforms is not a substantial concern. The waveforms we chose to replicate were taken from a series of waveforms along a 4mm length in the human carotid from either an AP or AG region. Therefore, the shear waveforms being generated by this new system, while they may not exactly match the chosen waveforms, are still representative, both in shear magnitude and waveform shape, of *in vivo* conditions. Conversely, the variation of shear at different radial distances is a significant concern. The desired range of

wall shear stress needs to be determined and then only cells that are cultured within the corresponding plate surface area should be collected for analysis. This will ensure more accurate and representative results.

The goal of this study was to develop an *in vitro* flow model to simulate shear stress patterns similar to those experienced by the endothelium in different regions of the vasculature and to evaluate the effects of this complex stimulus on EC response. In addition to these *in vivo* shear waveforms, this system will allow us to study the effects of: shear magnitude, fluctuations in shear values, rates of change of shear, and preconditioning with different shear waveforms. This will allow us to better elucidate the mechanisms by which ECs sense changes in blood flow patterns. These data further support observations that the endothelial cells can not only sense, but also discriminate among distinct shear stress stimuli. [1, 2] The data also demonstrate the utility of an arterial flow model to provide greater insight into the coordination of mechanisms involved in mechano-sensing in ECs. Ultimately, the extension of this method of analysis to endothelial phenotype in the natural disease context should provide valuable new insights into the links between endothelial dysfunction, hemodynamic forces, and atherogenesis.

APPENDIX A

Calculations

Table 1. Calculated shear stress values as they vary by increasing plate radius

cone angle (rad)	0.008726646
gap height (mm)	0.25

INPUT VALUES					**CONVERSIONS**		**CALCULATED VALUES**			
RPM	radius (mm)	viscosity (P)	kinematic viscosity (mm2/s)	height at radius (mm)	RPS	Rad/s	linear velocity (mm/s)	shear stress (dyne/cm2)	~R	shear rate
200	0	0.0078	0.7900	0.2540	3.3333	20.94	0.00	0.00	0.000	0.00
200	5	0.0078	0.7900	0.2976	3.3333	20.94	104.72	2.78	0.004	356.63
200	10	0.0078	0.7900	0.3413	3.3333	20.94	209.44	4.84	0.017	620.99
200	15	0.0078	0.7900	0.3849	3.3333	20.94	314.16	6.43	0.038	824.78
200	20	0.0078	0.7900	0.4285	3.3333	20.94	418.88	7.70	0.067	986.68
200	25	0.0078	0.7900	0.4722	3.3333	20.94	523.60	8.72	0.105	1118.40
200	30	0.0078	0.7900	0.5158	3.3333	20.94	628.32	9.58	0.151	1227.67
200	35	0.0078	0.7900	0.5594	3.3333	20.94	733.04	10.29	0.206	1319.76
200	40	0.0078	0.7900	0.6030	3.3333	20.94	837.76	10.91	0.269	1398.44

Table 2. Calculated shear stress values as they vary by increasing angular velocity

cone angle (rad)	0.008726646
gap height (mm)	0.25

INPUT VALUES					CONVERSIONS		CALCULATED VALUES		
RPM	radius (mm)	viscosity (P)	kinematic viscosity (mm2/s)	height at radius (mm)	RPS	Rad/s	linear velocity (mm/s)	shear stress (dyne/cm2)	~R
50	30	0.0078	0.7900	0.5158	0.8333	5.24	157.08	2.39	0.038
100	30	0.0078	0.7900	0.5158	1.6667	10.47	314.16	4.79	0.076
150	30	0.0078	0.7900	0.5158	2.5000	15.71	471.24	7.18	0.114
200	30	0.0078	0.7900	0.5158	3.3333	20.94	628.32	9.58	0.151
250	30	0.0078	0.7900	0.5158	4.1667	26.18	785.40	11.97	0.189
300	30	0.0078	0.7900	0.5158	5.0000	31.42	942.48	14.36	0.227
350	30	0.0078	0.7900	0.5158	5.8333	36.65	1099.56	16.76	0.265
400	30	0.0078	0.7900	0.5158	6.6667	41.89	1256.64	19.15	0.303
450	30	0.0078	0.7900	0.5158	7.5000	47.12	1413.72	21.55	0.341
500	30	0.0078	0.7900	0.5158	8.3333	52.36	1570.80	23.94	0.379
550	30	0.0078	0.7900	0.5158	9.1667	57.60	1727.88	26.33	0.416
600	30	0.0078	0.7900	0.5158	10.0000	62.83	1884.96	28.73	0.454
650	30	0.0078	0.7900	0.5158	10.8333	68.07	2042.04	31.12	0.492
700	30	0.0078	0.7900	0.5158	11.6667	73.30	2199.11	33.52	0.530
750	30	0.0078	0.7900	0.5158	12.5000	78.54	2356.19	35.91	0.568

APPENDIX B

Motion Programs

Motion program for continuous rotation (400 RPM) in one direction.

```
DEL CONT    ;Delete program, if any
DEF CONT    ;Begin definition of program
drive1      ;activate drive 1
scale0      ;disable scaling (program will use default values)
timst0      ;reset clock to zero, start clock
pset0       ;set position to zero
comexc1             ;activate continuous motion mode
mc1         ;enable continuous mode
l           ;start loop
timst0      ;reset clock to zero, start clock
;Point 1
d50000              ;set distance to 50000 steps (2 revolutions)
a80         ;set acceleration to 80 revolutions/sec/sec
v6.67       ;set velocity to 6.67 revolutions/sec
go1         ;start motion
ttim        ;output clock value
tpm         ;output motor position
ln          ;end loop
END         ;End program definition
```

Motion program for atheroprotective shear waveform with 5% dextran-70.

```
DEL LSHYS5      ;Delete program, if any
DEF LSHYS5      ;Begin definition of program
drive1
scale0
timst0
pset0
comexc1
mc1
l
timst0
a110
v2.77
go1
wait(tim=114)
ttim
ad115
v8.33
go1
wait(tim=196)
ttim
ad26
v3.5
go1
wait(tim=400)
ttim
a25
v3.82
go1
wait(tim=510)
ttim
ad16
v3.02
go1
wait(tim=610)
ttim
ad4
v2.63
go1
wait(tim=812)
ttim
tpm
ln
END             ;End program definition
```

Motion program for atherogenic shear waveform.

```
DEL OSH3        ;Delete program, if any
DEF OSH3        ;Begin definition of program
drive1          ;activate drive 1
scale0          ;disable scaling (program will use default values)
timst0          ;reset clock to zero, start clock
pset0           ;set position to zero
comexc1                 ;activate continuous motion mode
mc1             ;enable continuous mode
l               ;start loop
timst0          ;reset clock to zero, start clock
;Point 1
d50000                  ;set distance to 50000 steps (2 revolutions)
a80             ;set acceleration to 80 revolutions/sec/sec
v2              ;set velocity to 2 revolutions/sec
go1             ;start motion
wait(tim=30)    ;wait to execute next command until clock reaches 30milliseconds
ttim            ;output clock value
;2
d50000
ad91
v0
go1
wait(tim=60)
ttim
;3
d-50000
a125
v4.15
go1
wait(tim=94)
ttim
;4
d-50000
ad101
v0
go1
wait(tim=144)
ttim
;5
d50000
a58
v0.78
go1
wait(tim=170)
```

```
ttim
;6
d50000
ad30
v.01
go1
wait(tim=202)
ttim
;7
d-50000
a19
v.97
go1
wait(tim=262)
ttim
;8
d-50000
ad27
v0
go1
wait(tim=304)
ttim
;9
d50000
a13
v.83
go1
wait(tim=382)
ttim
;10
d50000
ad11
v0
go1
wait(tim=462)
ttim
;11
a3
v.5
go1
wait(tim=744)
ttim
;12
ad1.9
v.17
go1
```

```
wait(tim=978)
ttim
tpm             ;output motor position
ln              ;end loop
END             ;End program definition
```

APPENDIX C

Computational Fluid Dynamics

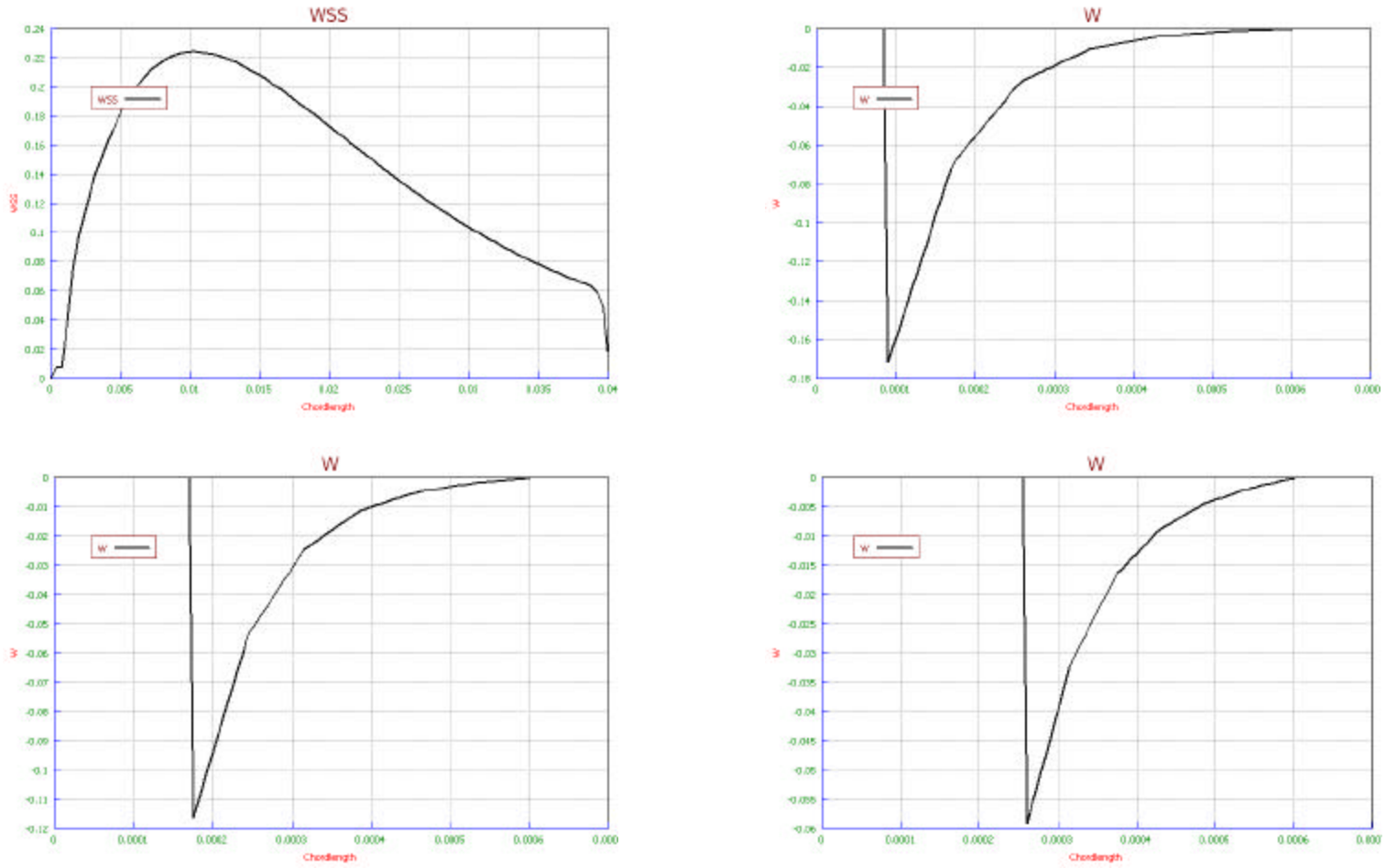

Figure 36. Wall shear stress (WSS) and tangential velocities (W) with respect to radial position (Chordlength) at time=0.01s after the start of the AG shear waveform.

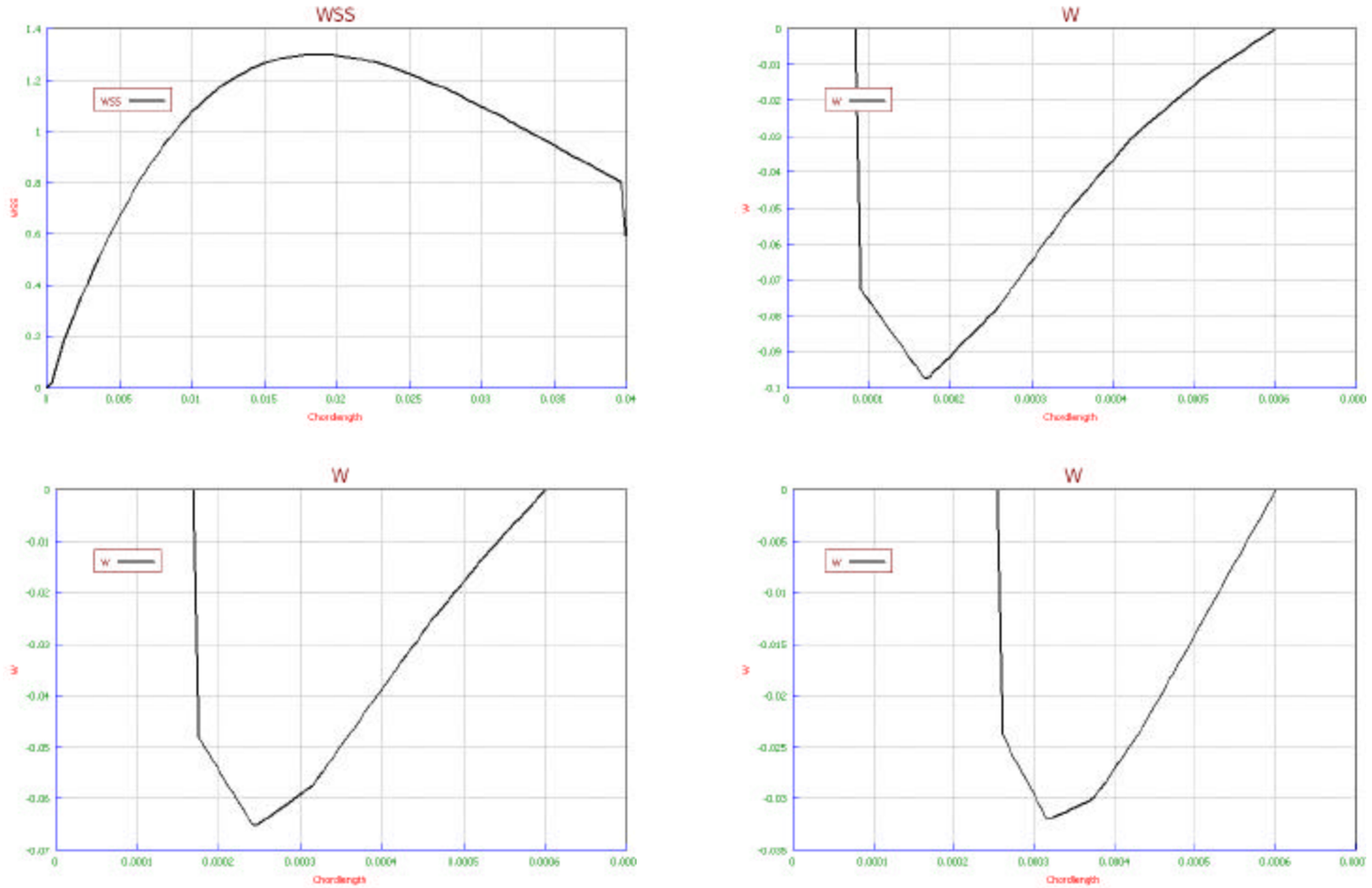

Figure 37. Wall shear stress (WSS) and tangential velocities (W) with respect to radial position (Chordlength) at time=0.04s after the start of the AG shear waveform. Velocity plots are at radius=3,2, and 1 cm, respectively.

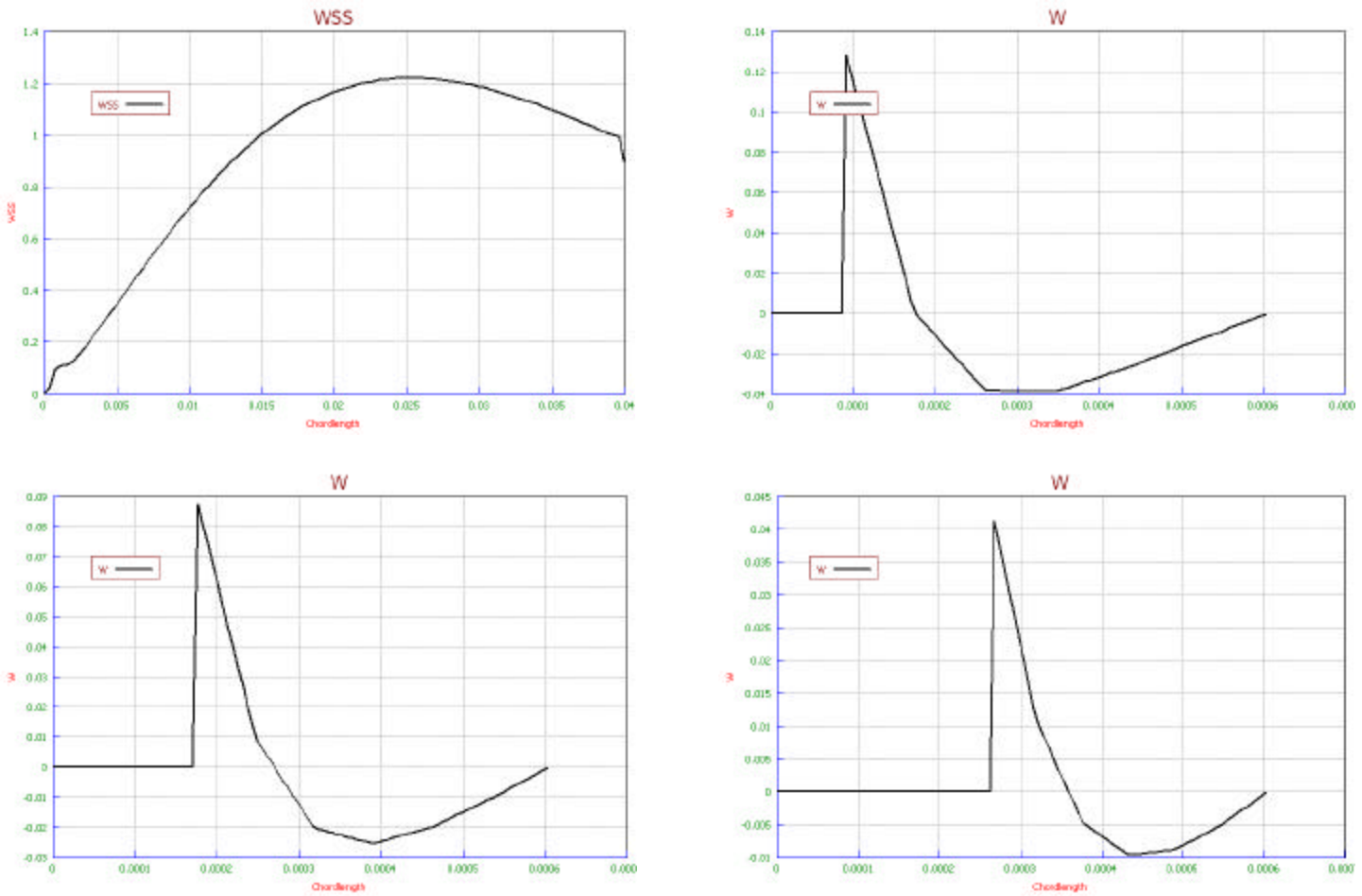

Figure 38. Wall shear stress (WSS) and tangential velocities (W) with respect to radial position (Chordlength) at time=0.05s after the start of the AG shear waveform. Velocity plots are at radius=3,2, and 1 cm, respectively.

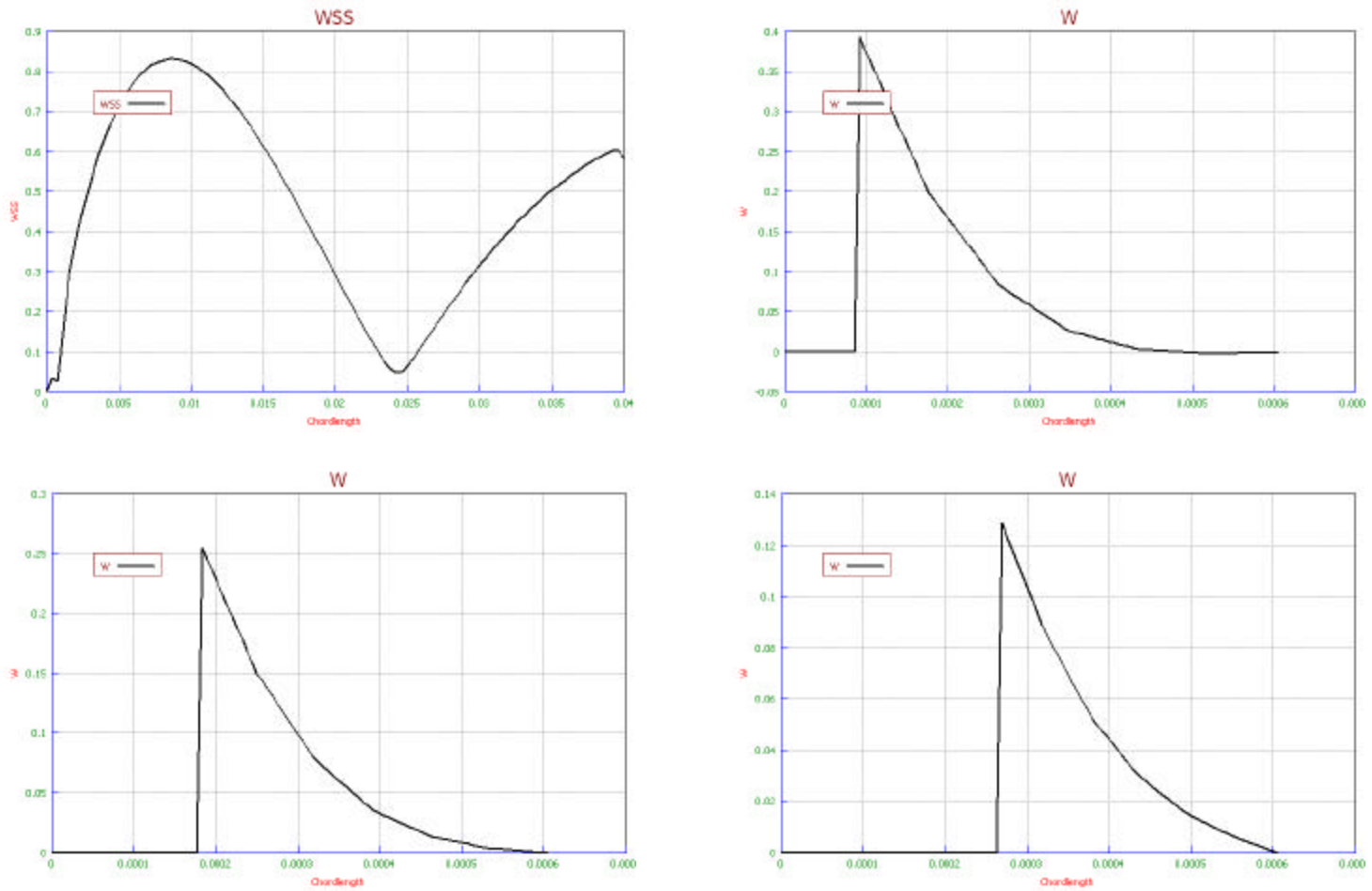

Figure 39. Wall shear stress (WSS) and tangential velocities (W) with respect to radial position (Chordlength) at time=0.07s after the start of the AG shear waveform. Velocity plots are at radius=3,2, and 1 cm, respectively.

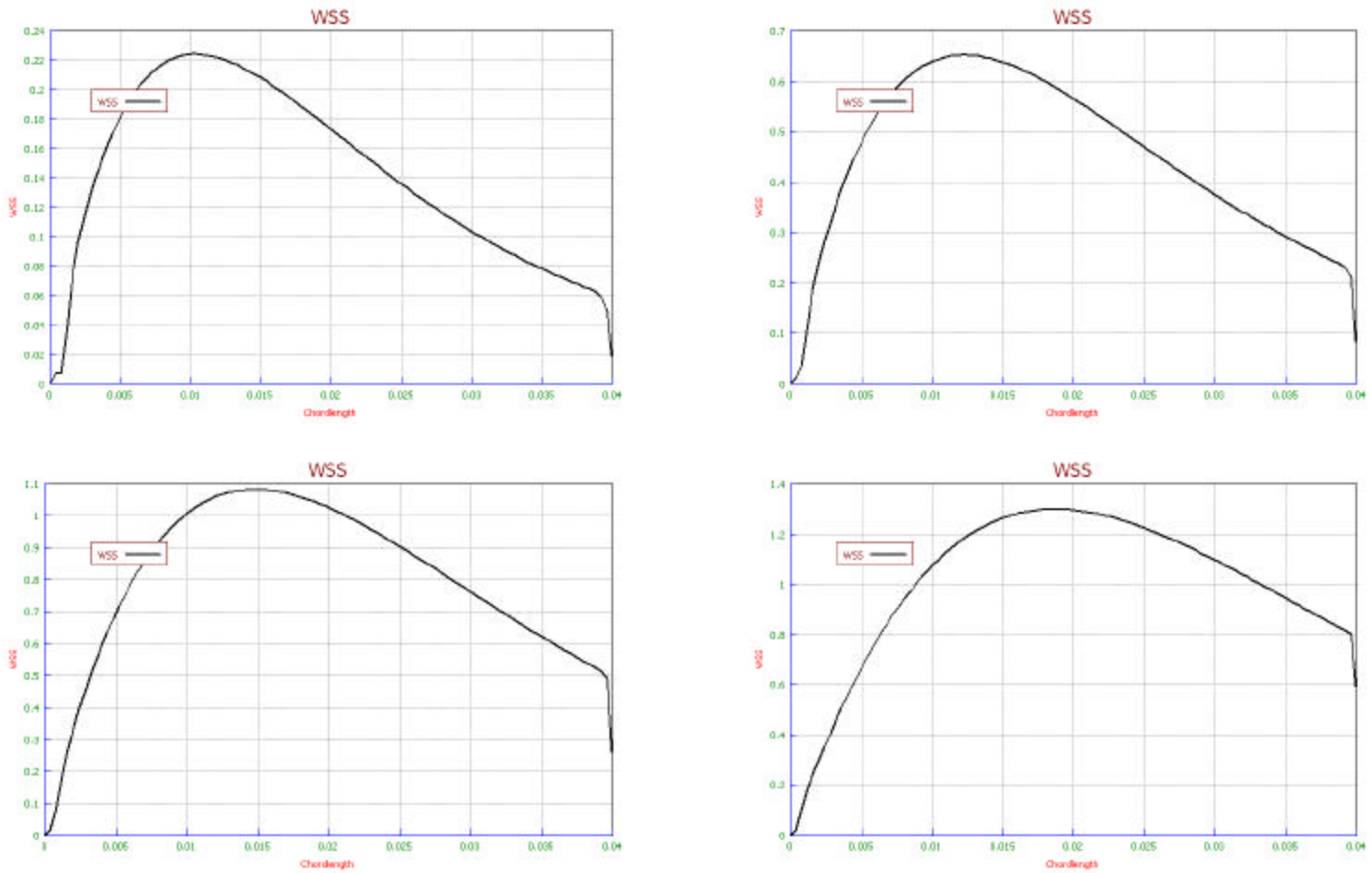

Figure 40. Wall shear stress (WSS) with respect to radial position (Chordlength) at time=0.01, 0.02, 0.03, and 0.04s after the start of the AG shear waveform, respectively.

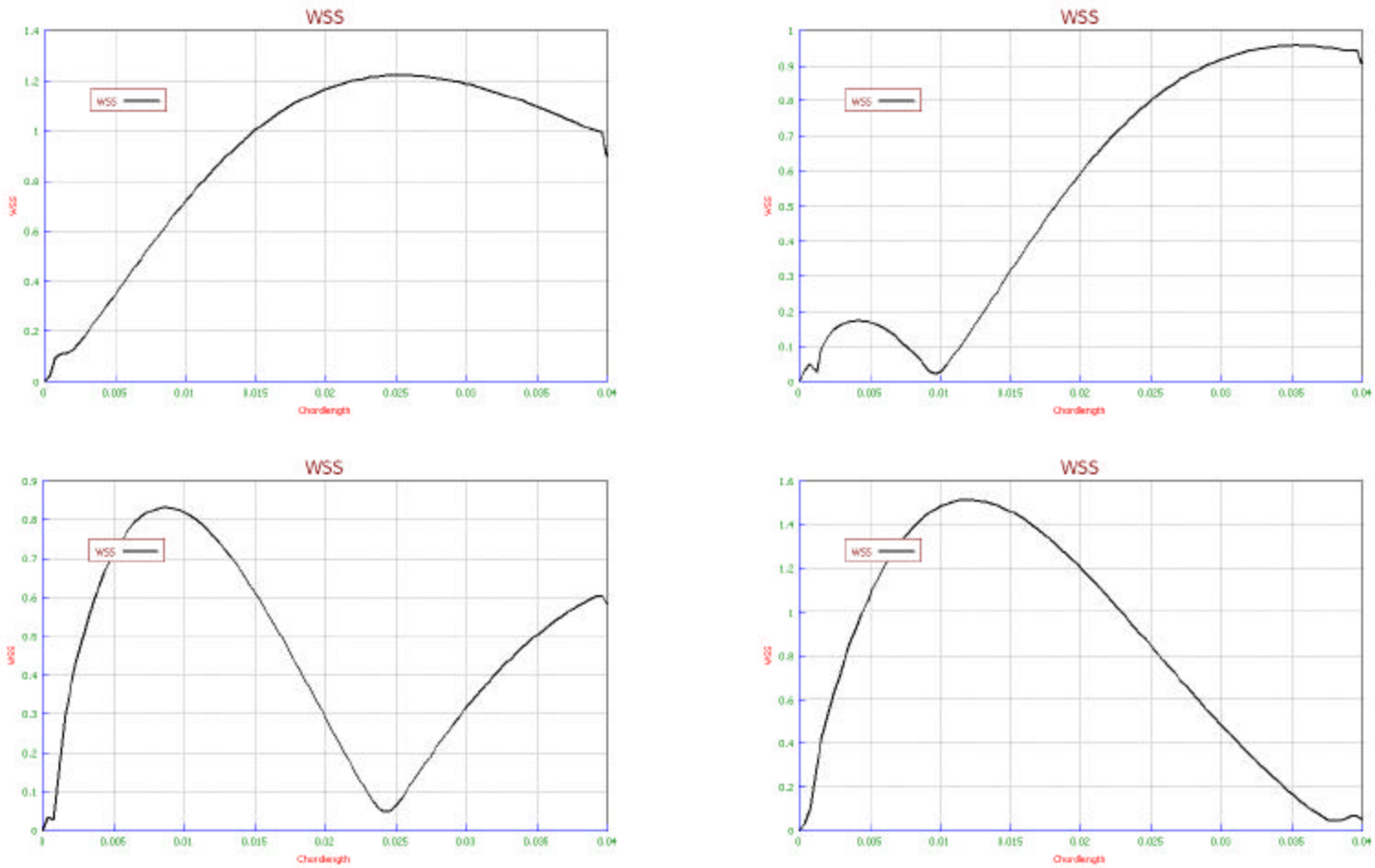

Figure 41. Wall shear stress (WSS) with respect to radial position (Chordlength) at time=0.05, 0.06, 0.07, and 0.08s after the start of the AG shear waveform, respectively.

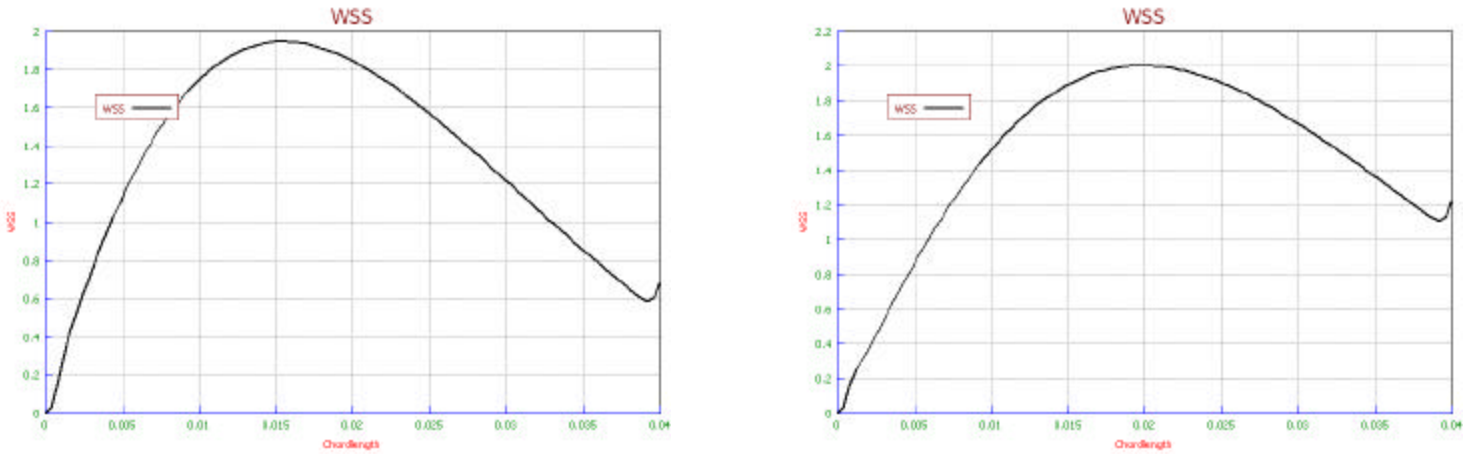

Figure 42. Wall shear stress (WSS) with respect to radial position (Chordlength) at time=0.09 and 0.1s after the start of the AG shear waveform, respectively.

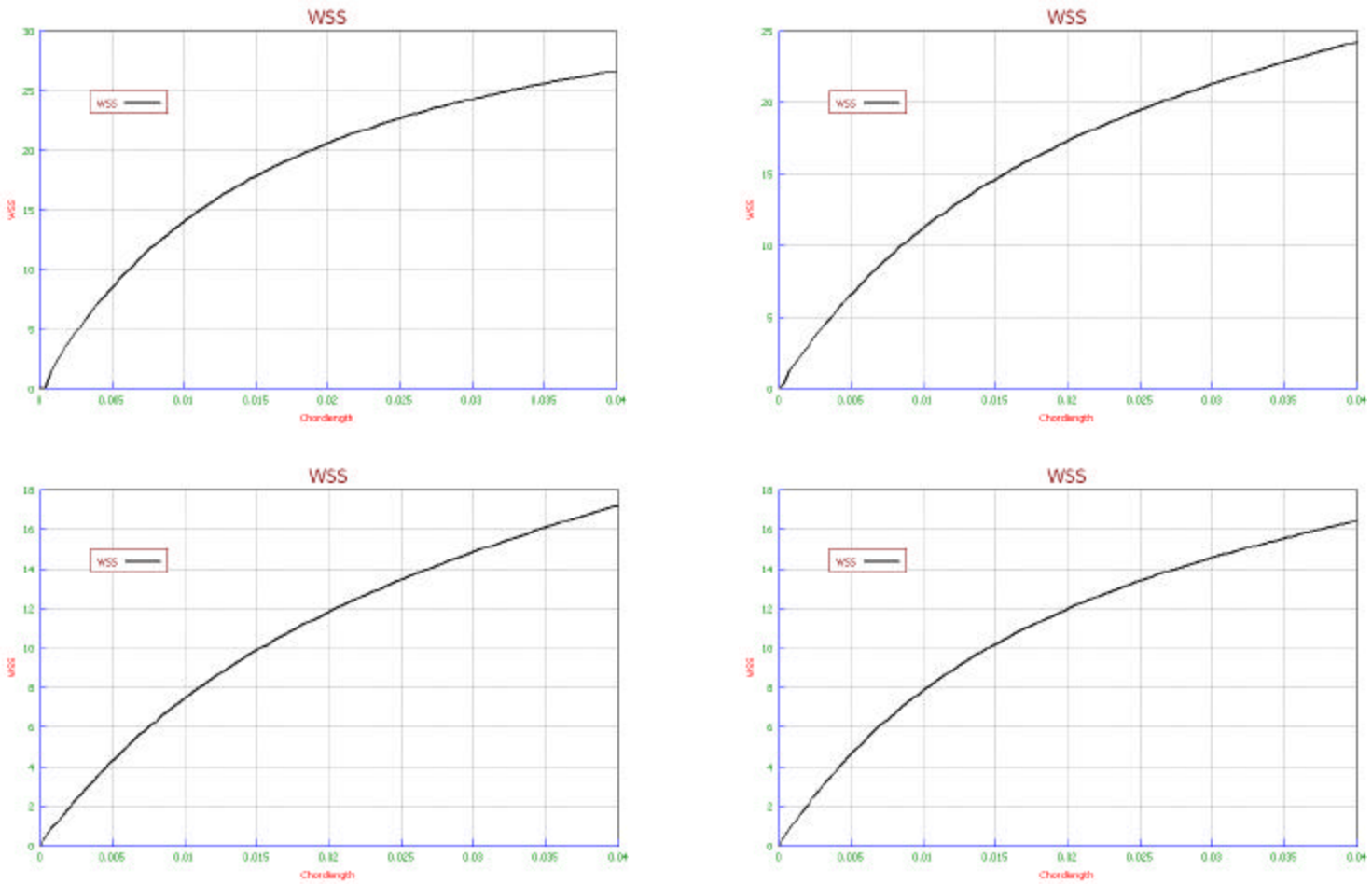

Figure 43. Wall shear stress (WSS) with respect to radial position (Chordlength) at time=0.1, 0.2, 0.3, and 0.4s after the start of the AG shear waveform, respectively.

REFERENCES

1. Bonow, R.O., et al., *World Heart Day 2002: the international burden of cardiovascular disease: responding to the emerging global epidemic.* Circulation, 2002. **106**(13): p. 1602-5.

2. Murray, C.J. and A.D. Lopez, *Mortality by cause for eight regions of the world: Global Burden of Disease Study.* Lancet, 1997. **349**(9061): p. 1269-76.

3. Association, A.H., *Heart Disease and Stroke Statistics — 2005 Update.* 2004.

4. Ross, R. and J.A. Glomset, *The pathogenesis of atherosclerosis (first of two parts).* N Engl J Med, 1976. **295**(7): p. 369-77.

5. Ross, R., *George Lyman Duff Memorial Lecture. Atherosclerosis: a problem of the biology of arterial wall cells and their interactions with blood components.* Arteriosclerosis, 1981. **1**(5): p. 293-311.

6. Friedman, M.H., et al., *Correlation between intimal thickness and fluid shear in human arteries.* Atherosclerosis, 1981. **39**(3): p. 425-36.

7. Ku, D.N., et al., *Pulsatile flow and atherosclerosis in the human carotid bifurcation. Positive correlation between plaque location and low oscillating shear stress.* Arteriosclerosis, 1985. **5**(3): p. 293-302.

8. Napoli, C., et al., *Fatty streak formation occurs in human fetal aortas and is greatly enhanced by maternal hypercholesterolemia. Intimal accumulation of low density lipoprotein and its oxidation precede monocyte recruitment into early atherosclerotic lesions.* J Clin Invest, 1997. **100**(11): p. 2680-90.

9. Ross, R., *The pathogenesis of atherosclerosis: a perspective for the 1990s.* Nature, 1993. **362**(6423): p. 801-9.

10. Glagov, S., et al., *Compensatory enlargement of human atherosclerotic coronary arteries.* N Engl J Med, 1987. **316**(22): p. 1371-5.

11. Dewey, C.F., Jr., et al., *The dynamic response of vascular endothelial cells to fluid shear stress.* J Biomech Eng, 1981. **103**(3): p. 177-85.

12. Giddens, D.P., C.K. Zarins, and S. Glagov, *The role of fluid mechanics in the localization and detection of atherosclerosis.* J Biomech Eng, 1993. **115**(4B): p. 588-94.

13. Nagel, T., et al., *Vascular endothelial cells respond to spatial gradients in fluid shear stress by enhanced activation of transcription factors.* Arterioscler Thromb Vasc Biol, 1999. **19**(8): p. 1825-34.

14. Davies, P.F., *Flow-mediated endothelial mechanotransduction.* Physiol Rev, 1995. **75**(3): p. 519-60.

15. Fuster, V., R. Ross, and E.J. Topol, *Atherosclerosis and coronary artery disease*. 1996, Philadelphia: Lippincott-Raven. 2 v. (xxv, 1661, 42).

16. Caro, C.G., J.M. Fitz-Gerald, and R.C. Schroter, *Atheroma and arterial wall shear. Observation, correlation and proposal of a shear dependent mass transfer mechanism for atherogenesis.* Proc R Soc Lond B Biol Sci, 1971. **177**(46): p. 109-59.

17. Fry, D.L., *Acute vascular endothelial changes associated with increased blood velocity gradients.* Circ Res, 1968. **22**(2): p. 165-97.

18. Krueger, J.W., D.F. Young, and N.R. Cholvin, *An in vitro study of flow response by cells.* J Biomech, 1971. **4**(1): p. 31-6.

19. Rosen, L.A., T.M. Hollis, and M.G. Sharma, *Alterations in bovine endothelial histidine decarboxylase activity following exposure to shearing stresses.* Exp Mol Pathol, 1974. **20**(3): p. 329-43.

20. DeForrest, J.M. and T.M. Hollis, *Shear stress and aortic histamine synthesis.* Am J Physiol, 1978. **234**(6): p. H701-5.

21. Nagel, T., et al., *Shear stress selectively upregulates intercellular adhesion molecule-1 expression in cultured human vascular endothelial cells.* J Clin Invest, 1994. **94**(2): p. 885-91.

22. Resnick, N., et al., *Platelet-derived growth factor B chain promoter contains a cis-acting fluid shear-stress-responsive element.* Proc Natl Acad Sci U S A, 1993. **90**(16): p. 7908.

23. Lin, M.C., et al., *Shear stress induction of the tissue factor gene.* J Clin Invest, 1997. **99**(4): p. 737-44.

24. Mondy, J.S., et al., *Platelet-derived growth factor ligand and receptor expression in response to altered blood flow in vivo.* Circ Res, 1997. **81**(3): p. 320-7.

25. McMillan, D.E., *Blood flow and the localization of atherosclerotic plaques.* Stroke, 1985. **16**(4): p. 582-7.

26. Nakashima, Y., et al., *Upregulation of VCAM-1 and ICAM-1 at atherosclerosis-prone sites on the endothelium in the ApoE-deficient mouse.* Arterioscler Thromb Vasc Biol, 1998. **18**(5): p. 842-51.

27. Levesque, M.J. and R.M. Nerem, *The elongation and orientation of cultured endothelial cells in response to shear stress.* J Biomech Eng, 1985. **107**(4): p. 341-7.

28. Muller, W.A., et al., *PECAM-1 is required for transendothelial migration of leukocytes.* J Exp Med, 1993. **178**(2): p. 449-60.

29. Rajavashisth, T.B., et al., *Induction of endothelial cell expression of granulocyte and macrophage colony-stimulating factors by modified low-density lipoproteins.* Nature, 1990. **344**(6263): p. 254-7.

30. Langille, B.L., M.A. Reidy, and R.L. Kline, *Injury and repair of endothelium at sites of flow disturbances near abdominal aortic coarctations in rabbits.* Arteriosclerosis, 1986. **6**(2): p. 146-54.

31. Shen, J., et al., *Fluid shear stress modulates cytosolic free calcium in vascular endothelial cells.* Am J Physiol, 1992. **262**(2 Pt 1): p. C384-90.

32. Olesen, S.P., D.E. Clapham, and P.F. Davies, *Haemodynamic shear stress activates a K+ current in vascular endothelial cells.* Nature, 1988. **331**(6152): p. 168-70.

33. White, G.E., M.A. Gimbrone, Jr., and K. Fujiwara, *Factors influencing the expression of stress fibers in vascular endothelial cells in situ.* J Cell Biol, 1983. **97**(2): p. 416-24.

34. Franke, R.P., et al., *Induction of human vascular endothelial stress fibres by fluid shear stress.* Nature, 1984. **307**(5952): p. 648-9.

35. Frangos, J.A., et al., *Flow effects on prostacyclin production by cultured human endothelial cells.* Science, 1985. **227**(4693): p. 1477-9.

36. Hollis, T.M. and L.A. Rosen, *Histidine decarboxylase activity of bovine aortic endothelium and intima-media.* Proc Soc Exp Biol Med, 1972. **141**(3): p. 978-81.

37. Diamond, S.L., S.G. Eskin, and L.V. McIntire, *Fluid flow stimulates tissue plasminogen activator secretion by cultured human endothelial cells.* Science, 1989. **243**(4897): p. 1483-5.

38. Davies, P.F., et al., *Turbulent fluid shear stress induces vascular endothelial cell turnover in vitro.* Proc Natl Acad Sci U S A, 1986. **83**(7): p. 2114-7.

39. Cinnamon, Y., et al., *The sub-lip domain--a distinct pathway for myotome precursors that demonstrate rostral-caudal migration.* Development, 2001. **128**(3): p. 341-51.

40. Traub, O. and B.C. Berk, *Laminar shear stress: mechanisms by which endothelial cells transduce an atheroprotective force.* Arterioscler Thromb Vasc Biol, 1998. **18**(5): p. 677-85.

41. Seebach, J., et al., *Endothelial barrier function under laminar fluid shear stress.* Lab Invest, 2000. **80**(12): p. 1819-31.

42. Resnick, N. and M.A. Gimbrone, Jr., *Hemodynamic forces are complex regulators of endothelial gene expression.* Faseb J, 1995. **9**(10): p. 874-82.

43. Gimbrone, M.A., Jr., et al., *Hemodynamics, endothelial gene expression, and atherogenesis.* Ann N Y Acad Sci, 1997. **811**: p. 1-10; discussion 10-1.

44. Topper, J.N. and M.A. Gimbrone, Jr., *Blood flow and vascular gene expression: fluid shear stress as a modulator of endothelial phenotype.* Mol Med Today, 1999. **5**(1): p. 40-6.

45. Glagov, S., et al., *Hemodynamics and atherosclerosis. Insights and perspectives gained from studies of human arteries.* Arch Pathol Lab Med, 1988. **112**(10): p. 1018-31.

46. Bussolari, S.R., C.F. Dewey, Jr., and M.A. Gimbrone, Jr., *Apparatus for subjecting living cells to fluid shear stress.* Rev Sci Instrum, 1982. **53**(12): p. 1851-4.

47. Boyd, N.L., et al., *Chronic shear induces caveolae formation and alters ERK and Akt responses in endothelial cells.* Am J Physiol Heart Circ Physiol, 2003. **285**(3): p. H1113-22.

48. Kubes, P., M. Suzuki, and D.N. Granger, *Nitric oxide: an endogenous modulator of leukocyte adhesion.* Proc Natl Acad Sci U S A, 1991. **88**(11): p. 4651-5.

49. Feigl, E.O., *EDRF--a protective factor?* Nature, 1988. **331**(6156): p. 490-1.

50. Steinberg, D., et al., *Beyond cholesterol. Modifications of low-density lipoprotein that increase its atherogenicity.* N Engl J Med, 1989. **320**(14): p. 915-24.

51. Wechezak, A.R., R.F. Viggers, and L.R. Sauvage, *Fibronectin and F-actin redistribution in cultured endothelial cells exposed to shear stress.* Lab Invest, 1985. **53**(6): p. 639-47.

52. Sato, M., M.J. Levesque, and R.M. Nerem, *Micropipette aspiration of cultured bovine aortic endothelial cells exposed to shear stress.* Arteriosclerosis, 1987. **7**(3): p. 276-86.

53. Sprague, E.A., et al., *Influence of a laminar steady-state fluid-imposed wall shear stress on the binding, internalization, and degradation of low-density lipoproteins by cultured arterial endothelium.* Circulation, 1987. **76**(3): p. 648-56.

54. Davies, P.F., et al., *Influence of hemodynamic forces on vascular endothelial function. In vitro studies of shear stress and pinocytosis in bovine aortic cells.* J Clin Invest, 1984. **73**(4): p. 1121-9.

55. Helmlinger, G., et al., *Effects of pulsatile flow on cultured vascular endothelial cell morphology.* J Biomech Eng, 1991. **113**(2): p. 123-31.

56. Thoumine, O., et al., *Elongation of confluent endothelial cells in culture: the importance of fields of force in the associated alterations of their cytoskeletal structure.* Exp Cell Res, 1995. **219**(2): p. 427-41.

57. DePaola, N., et al., *Vascular endothelium responds to fluid shear stress gradients.* Arterioscler Thromb, 1992. **12**(11): p. 1254-7.

58. Topper, J.N., et al., *Identification of vascular endothelial genes differentially responsive to fluid mechanical stimuli: cyclooxygenase-2, manganese superoxide dismutase, and endothelial cell nitric oxide synthase are selectively up-regulated by steady laminar shear stress.* Proc Natl Acad Sci U S A, 1996. **93**(19): p. 10417-22.

59. Garcia-Cardena, G., et al., *Biomechanical activation of vascular endothelium as a determinant of its functional phenotype.* Proc Natl Acad Sci U S A, 2001. **98**(8): p. 4478-85.

60. Gimbrone, M.A., Jr., et al., *Endothelial dysfunction, hemodynamic forces, and atherogenesis.* Ann N Y Acad Sci, 2000. **902**: p. 230-9; discussion 239-40.

61. Nichols, W.W., et al., *McDonald's blood flow in arteries: theoretic, experimental, and clinical principles*. 4th ed. 1997, London New York: Arnold; Oxford University Press. x, 564.

62. Hwang, N.H., et al., *Turbulent flow through a natural human mitral valve.* J Biomech, 1977. **10**(1): p. 59-67.

63. Frangos, J.A., T.Y. Huang, and C.B. Clark, *Steady shear and step changes in shear stimulate endothelium via independent mechanisms--superposition of transient and sustained nitric oxide production.* Biochem Biophys Res Commun, 1996. **224**(3): p. 660-5.

64. Owan, I., et al., *Mechanotransduction in bone: osteoblasts are more responsive to fluid forces than mechanical strain.* Am J Physiol, 1997. **273**(3 Pt 1): p. C810-5.

65. Wright, M., et al., *Effects of intermittent pressure-induced strain on the electrophysiology of cultured human chondrocytes: evidence for the presence of stretch-activated membrane ion channels.* Clin Sci (Lond), 1996. **90**(1): p. 61-71.

66. Benbrahim, A., et al., *A compliant tubular device to study the influences of wall strain and fluid shear stress on cells of the vascular wall.* J Vasc Surg, 1994. **20**(2): p. 184-94.

67. Moore, J.E., Jr., et al., *A device for subjecting vascular endothelial cells to both fluid shear stress and circumferential cyclic stretch.* Ann Biomed Eng, 1994. **22**(4): p. 416-22.

68. Ayajiki, K., et al., *Intracellular pH and tyrosine phosphorylation but not calcium determine shear stress-induced nitric oxide production in native endothelial cells.* Circ Res, 1996. **78**(5): p. 750-8.

69. Peng, X., et al., *In vitro system to study realistic pulsatile flow and stretch signaling in cultured vascular cells.* Am J Physiol Cell Physiol, 2000. **279**(3): p. C797-805.

70. Tseng, H., T.E. Peterson, and B.C. Berk, *Fluid shear stress stimulates mitogen-activated protein kinase in endothelial cells.* Circ Res, 1995. **77**(5): p. 869-78.

71. Ruel, J., et al., *Development of a parallel plate flow chamber for studying cell behavior under pulsatile flow.* Asaio J, 1995. **41**(4): p. 876-83.

72. Tardy, Y., et al., *Shear stress gradients remodel endothelial monolayers in vitro via a cell proliferation-migration-loss cycle.* Arterioscler Thromb Vasc Biol, 1997. **17**(11): p. 3102-6.

73. Dewey, C.F., Jr., *Effects of fluid flow on living vascular cells.* J Biomech Eng, 1984. **106**(1): p. 31-5.

74. Topper, J.N., et al., *Vascular MADs: two novel MAD-related genes selectively inducible by flow in human vascular endothelium.* Proc Natl Acad Sci U S A, 1997. **94**(17): p. 9314-9.

75. Buschmann, M.H., et al., *Analysis of flow in a cone-and-plate apparatus with respect to spatial and temporal effects on endothelial cells.* Biotechnol Bioeng, 2005. **89**(5): p. 493-502.

76. Fewell, M. and J.D. Hellums, *The secondary flow of Newtonian fluids in a cone-and-plate viscometer.* Trans. Soc. Rheol., 1977. **21**: p. 535-565.

77. Sdougos, H.P., *Secondary Flow and Turbulence in a Cone-and-Plate Couette-Flow Apparatus.* Bulletin of the American Physical Society, 1977. **22**(10): p. 1280-1280.

78. Sdougos, H.P., S.R. Bussolari, and C.F. Dewey, *Secondary Flow and Turbulence in a Cone-and-Plate Device.* Journal of Fluid Mechanics, 1984. **138**(Jan): p. 379-404.

79. Langille, L.B., *Integrity of arterial endothelium following acute exposure to high shear stress.* Biorheology, 1984. **21**(3): p. 333-46.

80. Schnittler, H.J., et al., *Improved in vitro rheological system for studying the effect of fluid shear stress on cultured cells.* Am J Physiol, 1993. **265**(1 Pt 1): p. C289-98.

81. Blackman, B.R., K.A. Barbee, and L.E. Thibault, *In vitro cell shearing device to investigate the dynamic response of cells in a controlled hydrodynamic environment.* Ann Biomed Eng, 2000. **28**(4): p. 363-72.

82. Dai, G., et al., *Distinct endothelial phenotypes evoked by arterial waveforms derived from atherosclerosis-susceptible and -resistant regions of human vasculature.* Proc Natl Acad Sci U S A, 2004. **101**(41): p. 14871-6.

83. Hollis, T.M. and R.A. Ferrone, *Effects of shearing stress on aortic histamine synthesis.* Exp Mol Pathol, 1974. **20**(1): p. 1-10.

84. Jo, H., et al., *Differential effect of shear stress on extracellular signal-regulated kinase and N-terminal Jun kinase in endothelial cells. Gi2- and Gbeta/gamma-dependent signaling pathways.* J Biol Chem, 1997. **272**(2): p. 1395-401.

85. Go, Y.M., et al., *Protein kinase B/Akt activates c-Jun NH(2)-terminal kinase by increasing NO production in response to shear stress.* J Appl Physiol, 2001. **91**(4): p. 1574-81.

86. Rieder, M.J., et al., *Suppression of angiotensin-converting enzyme expression and activity by shear stress.* Circ Res, 1997. **80**(3): p. 312-9.

87. Silkworth, J.B. and W.E. Stehbens, *Shape of Endothelial Cells in En-Face Preparations of Rabbit Blood-Vessels.* Angiology, 1975. **26**(6): p. 474-487.

88. Langille, B.L. and S.L. Adamson, *Relationship between blood flow direction and endothelial cell orientation at arterial branch sites in rabbits and mice.* Circ Res, 1981. **48**(4): p. 481-8.

89. Blackman, B.R., G. Garcia-Cardena, and M.A. Gimbrone, Jr., *A new in vitro model to evaluate differential responses of endothelial cells to simulated arterial shear stress waveforms.* J Biomech Eng, 2002. **124**(4): p. 397-407.

90. Nishida, K., et al., *Molecular cloning and characterization of the constitutive bovine aortic endothelial cell nitric oxide synthase.* J Clin Invest, 1992. **90**(5): p. 2092-6.

91. Rubanyi, G.M., J.C. Romero, and P.M. Vanhoutte, *Flow-induced release of endothelium-derived relaxing factor.* Am J Physiol, 1986. **250**(6 Pt 2): p.H1145-9.

92. Kuchan, M.J. and J.A. Frangos, *Role of calcium and calmodulin in flow-induced nitric oxide production in endothelial cells.* Am J Physiol, 1994. **266**(3 Pt 1): p. C628-36.

93. Sessa, W.C., et al., *Chronic exercise in dogs increases coronary vascular nitric oxide production and endothelial cell nitric oxide synthase gene expression.* Circ Res, 1994. **74**(2): p. 349-53.

94. Corson, M.A., et al., *Phosphorylation of endothelial nitric oxide synthase in response to fluid shear stress.* Circ Res, 1996. **79**(5): p. 984-91.

95. Boo, Y.C. and H. Jo, *Flow-dependent regulation of endothelial nitric oxide synthase: role of protein kinases.* Am J Physiol Cell Physiol, 2003. **285**(3): p. C499-508.

96. Boo, Y.C., et al., *Shear stress stimulates phosphorylation of eNOS at Ser(635) by a protein kinase A-dependent mechanism.* Am J Physiol Heart Circ Physiol, 2002. **283**(5): p. H1819-28.

97. Sorescu, G.P., et al., *Bone morphogenic protein 4 produced in endothelial cells by oscillatory shear stress induces monocyte adhesion by stimulating reactive oxygen species production from a nox1-based NADPH oxidase.* Circ Res, 2004. **95**(8): p. 773-9.

98. Sorescu, G.P., et al., *Bone morphogenic protein 4 produced in endothelial cells by oscillatory shear stress stimulates an inflammatory response.* J Biol Chem, 2003. **278**(33): p. 31128-35.

99. Oshinski, J.N., et al., *Determination of wall shear stress in the aorta with the use of MR phase velocity mapping.* J Magn Reson Imaging, 1995. **5**(6): p. 640-7.

100. Oyre, S., et al., *In vivo wall shear stress measured by magnetic resonance velocity mapping in the normal human abdominal aorta.* Eur J Vasc Endovasc Surg, 1997. **13**(3): p. 263-71.

101. Helmlinger, G., B.C. Berk, and R.M. Nerem, *Calcium responses of endothelial cell monolayers subjected to pulsatile and steady laminar flow differ.* Am J Physiol, 1995. **269**(2 Pt 1): p. C367-75.

102. Papapetropoulos, A., R.D. Rudic, and W.C. Sessa, *Molecular control of nitric oxide synthases in the cardiovascular system.* Cardiovasc Res, 1999. **43**(3): p. 509-20.

103. Rudic, R.D., et al., *Direct evidence for the importance of endothelium-derived nitric oxide in vascular remodeling.* J Clin Invest, 1998. **101**(4): p. 731-6.